

GPO PRICE \$ \_\_\_\_\_

CFSTI PRICE(S) \$ \_\_\_\_\_

Hard copy (HC) 3.00

Microfiche (MF) 1.75

ff 653 July 65

FACILITY FORM 502

**N66 29371**

(ACCESSION NUMBER)

76

(PAGES)

TMX-56814

(NASA CR OR TMX OR AD NUMBER)

(THRU)

(CODE)

07

(CATEGORY)

# RADIATION PATTERNS AND ADMITTANCE OF AN AXIAL SLOT

## ON A PLASMA COVERED CYLINDER

C. M. Knop  
Andrew Corporation  
Orland Park, Illinois

C. T. Swift  
NASA Langley Research Center  
Langley Station, Hampton, Va.

H. Hodara  
National Engineering Science Company  
Pasadena, California

Presented at the 3rd Symposium on the Plasma Sheath  
Plasma Electromagnetics of Hypersonic Flight

Boston, Massachusetts  
September 21-23, 1965

RADIATION PATTERNS AND ADMITTANCE OF AN AXIAL SLOT  
ON A PLASMA COVERED CYLINDER\*

\*This work was partially supported by Contract NAS1-4623

C. M. Knop<sup>†</sup>  
Andrew Corporation  
Orland Park, Illinois

<sup>†</sup>Formerly of NESCO, Pasadena, California

C. T. Swift  
NASA Langley Research Center  
Langley Station, Hampton, Va.

H. Hodara  
National Engineering Science Company  
Pasadena, California

INTRODUCTION

The admittance characteristics of three types of slotted-cylinder antennas are considered, namely, the long axial slot, the finite axial slot, and the gap antenna backed by a short-circuited radial cavity.

Most of the present effort is confined to a study of the long slot on the cylinder. This was done because the computational requirements are not too severe, yet the results should be indicative of the trends experienced by finite apertures in a reentry environment. Systematic computations of the admittance per unit length are made for various coating conditions.

First, the case of no coating is considered, and results are compared with those for identical slots on flat ground planes. Second, the special case of the plasma resonant  $\omega = \omega_p$ ,  $\nu = 0$  coating is analyzed to determine whether or not a measurement of the input admittance at resonance will yield diagnostic information. Finally, the case of a general coating is treated to ascertain the effects of losses and plasma inhomogeneities on the admittance.

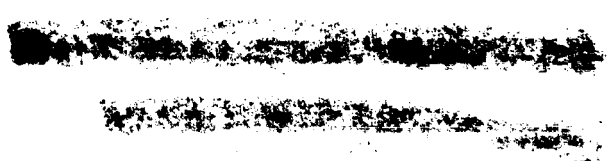
The exterior portion of finite apertures on coated cylinders are not too difficult to analyze but can lead to computational difficulties, even in the far field where asymptotic expansions may be made to simplify the field expressions. In the near field, no such expansions are allowed; therefore, the computational requirements of the external admittance are more severe. Furthermore, the size of the cylinder chosen for the present analysis (based on adaptability to feed with the slotted line) was so large that additional difficulties were introduced into the computations due to the large arguments of the Bessel and Hankel functions involved.

The work on the large cylinder includes specific computations of the conductance for the uncoated cylinder, and experimental results for both coated and uncoated cylinders. Admittance expressions for the coated cylinder are given and preliminary calculations of the conductance are discussed. Experimental and theoretical results for radiation patterns are also discussed.

Finally, the gap antenna, backed by a short circuited radial cavity and fed by a current element at the periphery is briefly discussed. Specific computations of the impedance for the case of no coating are made, and expressions with coating are given.

#### THE INFINITE SLOT ON A COATED CYLINDER

The geometry of the structure considered is shown in figure 1. A long slot is cut into an infinite conducting cylinder, and is excited by an electric field which is uniform along the axis, and across the slot, and which varies in time as  $e^{+j\omega t}$ . The structure is coated with a dielectric, whose complex index of refraction,  $N$  may vary in the radial direction.



The tangential fields,  $H_z$  and  $E_\phi$ , at any point exterior to the cylinder are described by a Fourier series in azimuth, i.e.,

$$H_z(\rho, \phi) = \sum_{m=-\infty}^{\infty} \bar{H}_{mz}(\rho) e^{-jm\phi} \quad (1a)$$

$$E_\phi(\rho, \phi) = \sum_{m=-\infty}^{\infty} \bar{E}_{m\phi}(\rho) e^{-jm\phi} \quad (1b)$$

Note that equations (1) are independent of the axial coordinate, and that the modal coefficients  $\bar{H}_{mz}(\rho)$  and  $\bar{E}_{m\phi}(\rho)$  depend only on the radial coordinate. These coefficients are determined by a straightforward application of the boundary conditions (appendix II).

The complex power per unit length radiated from the aperture is found by integrating the radial component of the Poynting vector across the slot, i.e.,

$$P = \int_{-\phi_0/2}^{\phi_0/2} S_{\rho a} d\phi = \frac{a}{2} \int_{-\phi_0/2}^{\phi_0/2} E_\phi^*(a, \phi) H_z(a, \phi) d\phi \quad (2)$$

The substitution of equations (1) into equation (2) gives

$$\begin{aligned} P &= \frac{a}{2} \sum_{m'=-\infty}^{\infty} \sum_{m=-\infty}^{\infty} \bar{E}_{m'\phi}^*(a) \bar{H}_{mz}(a) \int_{-\pi}^{\pi} e^{-j(m-m')\phi} d\phi \\ &= \pi a \sum_{m'=-\infty}^{\infty} \sum_{m=-\infty}^{\infty} \bar{E}_{m'\phi}^*(a) \bar{H}_{mz}(a) \delta_m^{m'} = \pi a \sum_{m=-\infty}^{\infty} \bar{E}_{m\phi}^*(a) \bar{H}_{mz}(a) \end{aligned} \quad (3)$$

which is nothing more than Parseval's theorem in cylindrical coordinates.<sup>1</sup>



The external or radiation admittance is defined by<sup>2</sup>

$$Y_{cl} = \frac{2P}{|V_o|^2} = 2\pi a \sum_{m=-\infty}^{\infty} \frac{\bar{E}_{m\phi}^*(a) \bar{E}_{mz}(a)}{|V_o|^2} \quad (4)$$

where  $V_o$  is the applied potential across the slot. Suppose, now that the slot is fed by a parallel-plate waveguide excited in the TEM mode. It is assumed that all higher modes are negligible so that  $E_\eta$  is the only component of tangential electric field across the aperture, and is of the form

$$E_\eta = \frac{V_o}{a} \quad (5)$$

If the slot is sufficiently thin, then  $E_\eta \cong E_\phi$  and  $d_\eta \cong a d\phi$ . Therefore the following transform pair exists:

$$E_\eta \cong E_\phi = \frac{V_o}{a}$$

$$E_{m\phi} = \frac{V_o}{2\pi a} \frac{\sin m\phi_o/2}{m\phi_o/2} \quad (6b)$$

Having specified the electric field at the aperture, the external admittance may be computed.

#### NO COATING

If the antenna radiates into free space, the normalized external admittance per unit length as derived in appendix II is

$$\lambda_v Y_{cvl} = \frac{Y_{cvl} \lambda_v}{Y_o} = \frac{-j2}{\pi C} \sum_{m=0}^{\infty} \frac{a_m}{(1 + \delta_o^m)} \frac{H_m^{(2)}(C)}{H_m^{(2)'}(C)} \quad (7)$$

Equation (7) was programed on an electronic computer and results were obtained for two cylinders having different gaps whose circumference-to-wavelength ratio ranged from 8.4 to 45.4. The results are given in

figure 2. For reference, the admittance of a slot of the same width on a flat ground plane as given by Harrington<sup>3</sup> is also plotted in figure 2. To the accuracy with which one could read Harrington's graph, the admittance of the slot on the cylinder throughout the whole range of  $C$  was very close to that of a slot on a flat ground plane.

#### RESONANT COATING

It has been shown (ref. 4) that only the  $m = 0$  mode is supported at the plasma resonant condition,  $N = 0$ , (i.e.,  $\nu = 0$ ,  $\omega_p = \omega$ ); therefore, the radiation patterns of an infinitely long slot (or the equatorial patterns of a finite slot) are circular, regardless of the size of the cylinder and thickness of the sheath as long as each are finite. Since the sudden deformation of the radiation pattern into a circle suggests a method of diagnosing a reentry plasma, the admittance was also investigated to determine its behavior at plasma resonance for possible means of diagnostics. At the resonant condition, this admittance per unit length (appendix II) is:

$$Y_{Rl} \lambda_v = \frac{Y_{Rl} \lambda_v}{Y_0} \Big|_{W>1} = -j \frac{1}{CW \left[ \frac{H_0^{(2)'}(C)}{H_0^{(2)}(C)} + \frac{C}{2} \left( W - \frac{1}{W} \right) \right]} \quad (8)$$

The results of equation (8) are plotted in figure 3 as a function of  $C$  and  $W$ . Again two cylinders were chosen with  $C$  ranging between 8.4 and 45.4. Note that for  $W = 1.00 + \epsilon$ , which corresponds to a vanishing plasma thickness, the conductance decreases from the free-space value by an order of magnitude. Also, the susceptance can change from a large capacitive to a small inductive value or zero when the structure is

coated with this resonant plasma. As the plasma becomes thicker, the admittance per unit length approaches zero. This tendency for the admittance to drop at resonance suggests that a measurement of admittance could also be used for diagnostics.

The admittance of the slot has not yet been computed as the index of refraction increases from zero to some small finite value. However, based upon calculated changes in the radiation patterns due to a small departure from resonance,<sup>4</sup> one concludes that additional azimuthal modes ( $m = 1, 2, 3$ , etc.) are rapidly introduced into the field dependence, at least for  $C$  ranging between 22.7 and 45.4. As such, one can expect that these modes will alter, perhaps significantly, the input admittance from what it is at resonance; the extent of the alteration increasing with increasing  $C$ . However, for small  $C$ , this alteration may still be sufficiently small to cause a measurement of the input admittance near and at plasma resonance to be a useful plasma diagnostic tool. This remains to be investigated.

#### GENERAL COATING

The method described by Swift<sup>5</sup> was used to analyze the slotted cylinder coated with a dielectric having a complex index of refraction. In this approach, the wave equation is numerically integrated through the plasma, thereby avoiding the computational problem of evaluating Bessel and Hankel functions of complex arguments, which describe the functional behavior of the fields within the coating. Furthermore, if this method is used, the case of a coating whose dielectric properties vary radially may also be treated.

Using Swift's notation, the normalized admittance for either homogeneous or inhomogeneous coatings (see appendix II for an outline) is:

$$Y_{cl} = \frac{Y_{cl}\lambda_v}{Y_0} = -j \frac{2}{a} \frac{\epsilon(a)}{\epsilon_0} \sum_{m=0}^{\infty} a_m \frac{t_m(a) + ju_m(a)}{t_m'(a) + ju_m'(a)} \quad (9)$$

where the prime indicates differentiation with respect to the radial parameter.

Computations of equation (9) are plotted in figures 5 and 6 as a function of complex index of refraction for coating thickness corresponding to  $\frac{2\pi(b-a)}{\lambda_v} = 0.25$  and a slot width corresponding to  $\frac{2\pi w}{\lambda_v} = 0.25$  for cylinders of size  $C = 4, 8, \text{ and } 12$ . It is important to note that the admittance is relatively insensitive to variations in  $C$ . One is therefore tempted to conclude that the admittance of identical slots on cylinders and flat ground planes are, for all practical purposes, the same\* if  $C \geq 4$  and if the loss angle  $\delta$  of the coating is between  $90^\circ$  and  $180^\circ$ , and if the magnitude of  $N \geq 1$ .

Flow field analysis shows that the electron density and collision frequency may vary considerably within the plasma sheath. A typical example of the distribution along a normal to the vehicle is shown in figure 7, and was chosen as a coating for a cylinder of physical radius 4.152 cm and an aperture width of 1.016 cm<sup>†</sup>. The admittance was computed as a function of the exciting frequency, and the results are given in figure 8.

---

\*A more general conjecture of this type was suggested during conversations with one of the writers (CMK) by W. Rotman of AFCRL prior to the time these extensive computations were performed.

<sup>†</sup>This width corresponds to the width of a standard X-band waveguide.

Nineteen admittance points were computed in the frequency interval of 10.0 to 11.8 kmc, yet this number was insufficient to establish a smooth curve because of small-scale fluctuations. Nonetheless, some interesting features are revealed. The most striking effect occurs in the region of peak plasma frequency (10.76 kmc), where the conductance decreases sharply and susceptance begins to decrease monotonically.

This seems to be consistent with the results of the resonant plasma coating. At frequencies above resonance, the conductance rises rapidly, but the susceptance remains relatively constant. As the frequency increases, the admittance should approach the no coating values. Below resonance, the curves are fluctuating too much to suggest any general conclusions.

For the types of distributions shown in figure 7, the peak plasma frequency seems to be a sharp dividing point for the admittance properties of slots on cylinders. Whether this is true in general remains to be seen.

#### THE AXIAL SLOT ON A COATED CYLINDER

The geometry is shown in figure 9. A waveguide, excited in the  $TE_{01}$  mode opens onto a cylindrical ground plane, with the long dimension of the waveguide parallel to the axis of the cylinder. Higher-order modes are neglected in the waveguide, and the slot is assumed to be thin enough so that over the slot  $E_\eta = E_\phi$  and  $a d\phi = d\eta$ .

Since the aperture is finite, and since the tangential fields vary with  $z$ , the fields are described by continuous modes in axis and discrete modes in azimuth, i.e.,

$$H_z(\rho, \phi, z) = \sum_{m=-\infty}^{\infty} \int_{-\infty}^{\infty} \bar{H}_{mz}(\rho) e^{-jhz} e^{-jm\phi} dh \quad (10a)$$

$$E_{\phi}(\rho, \phi, z) = \sum_{m=-\infty}^{\infty} \int_{-\infty}^{\infty} \bar{\bar{E}}_{m\phi}(\rho) e^{-jh_z z} e^{-jm\phi} dh \quad (10b)$$

And the complex power radiated by the aperture is

$$P = \frac{1}{2} \int_{-z_0/2}^{z_0/2} \int_{-\phi_0/2}^{\phi_0/2} E_{\phi}^*(a, \phi, z) H_z(a, \phi, z) a \, d\phi \, dz \quad (11)$$

Using Parseval's theorem, equation (11) can be rewritten in the following form

$$P = \frac{1}{2} (2\pi)^2 a \sum_{m=-\infty}^{\infty} \int_{-\infty}^{\infty} \bar{\bar{E}}_{m\phi}^*(a) \bar{\bar{H}}_{mz}(a) dh \quad (12)$$

And, the external admittance is:

$$Y_c = \frac{2P}{|V_0|^2} = 4\pi^2 a \sum_{m=-\infty}^{\infty} \int_{-\infty}^{\infty} \frac{\bar{\bar{E}}_{m\phi}^*(a) \bar{\bar{H}}_{mz}(a)}{|V_0|^2} dh \quad (13)$$

If the tangential field is  $E_{\eta} \cong E_{\phi}$  the following transform pair exists:

$$E_{\phi}(a, \phi, z) = \frac{V_0}{w} \cos\left(\frac{\pi z}{l}\right) \quad (14a)$$

$$\bar{\bar{E}}_{m\phi}(a) = \frac{-V_0}{2\pi a} \frac{\cos\left(\frac{hl}{2}\right)}{l \left(h^2 - \frac{\pi^2}{l^2}\right)} \frac{\sin(m\phi_0/2)}{(m\phi_0/2)} \quad (14b)$$

The external admittance can now be computed using equations (13) and (14b) in connection with the solution of the boundary-value problem, which gives  $\bar{\bar{H}}_{mz}(a)$ .

NO COATING

For this case of no coating, the normalized external conductance and susceptance are

$$g_{cv} = \frac{G_{cv}}{Y_0} = \frac{1}{2\pi^5 k^4 p^2} \sum_{m=0}^{\infty} \frac{a_m}{(1 + \delta_0^m)} I_{mg} \quad (15a)$$

$$b_{cv} = \frac{B_{cv}}{Y_0} = \frac{1}{2\pi^3 p k^3} \sum_{m=0}^{\infty} \frac{a_m}{(1 + \delta_0^m)} (I_{1m} - I_{2m}) \quad (15b)$$

where

$$I_{mg} = \int_0^1 \frac{\cos^2(\pi k y) dy}{\left(y^2 - \frac{1}{4k^2}\right)^2 \left|H_m(2)' \left[2\pi p k \sqrt{1 - y^2}\right]\right|^2} \quad (16a)$$

$$I_{1m} = \int_1^{\infty} \frac{\sqrt{y^2 - 1} \cos^2(\pi k y) K_m \left[2\pi p k \sqrt{y^2 - 1}\right] dy}{\left(y^2 - \frac{1}{4k^2}\right)^2 K_m' \left[2\pi p k \sqrt{y^2 - 1}\right]} \quad (16b)$$

$$I_{2m} = \int_0^1 \frac{\sqrt{1 - y^2} \cos(\pi k y) \{J_m(x) J_m'(x) + Y_m(x) Y_m'(x)\} dy}{\left(y^2 - \frac{1}{4k^2}\right)^2 \left|H_m(2)'(x)\right|^2} \quad (16c)$$

Equation (15a) was computed over the X-band range of 6.56 to 13.12 kmc corresponding to a range of slot lengths of  $1/2$  to 1 wavelength for the  $TE_{01}$  mode, and the results are shown in figure 10. For this range of frequencies and the 13-inch-diameter cylinder used ( $2a = 13$  in.) the parameter  $C$  increases from 22.7 at  $k = 0.5$  to 45.4 at  $k = 1.0$ .

As a partial check of the computations, the width of the slot at  $k = 0.5$  was allowed to approach zero in order to compare the results with those of Wait (ref. 5) for the thin resonant slot. The computations performed here give  $g_{cv} = 0.383$  compared to Wait's  $g_{cv}|_{\text{Wait}} = 0.384$ . This partial check served as a go-ahead for proceeding with the other cases.

## EXPERIMENTAL RESULTS - NO COATING

The particular size of aperture and range of cylinder size  $C$  considered in most of the computations were chosen with X-band experiments in mind. The cylinder shown in figure 11 is 13 inches in diameter and 24 inches long, and is just large enough to contain a Hewlett-Packard slotted line. The aperture size is 0.4 inch  $\times$  0.9 inch, which corresponds to the inner dimensions of a standard RG-52U waveguide. The short circuit was realized by placing a small brass plate curved to fit the cylinder surface and held in place by a strap. Photographs of the end view showing the feed arrangement and the measurement setup is shown in figures 11 and 12.

The experimental and theoretical results are shown in figure 13. The measured and calculated values of the input conductance differ by, at most, 5 percent. The agreement is sufficiently close to conclude that the effect of higher-order modes and/or computational errors are negligible for the large-sized uncoated cylinder used here. Agreement between first-order theory and experiment can also be expected to be good for smaller cylinders with correspondingly thinner slots.

## EXPERIMENTAL RESULTS - POLYETHYLENE COATING

The cylinder used above for the noncoated condition was coated with a polyethylene coating (representing, electrically, an ablative coating) of a quarter-inch thickness, i.e.,  $T = b - a = 0.25$  inch, and measurements of input waveguide admittance were made. The dielectric constant of this coating material was first measured over the X-band frequency range to ascertain the correctness of the published value of  $\epsilon_r = 2.25$ . Four samples were cut out of the polyethylene stock sheet and their dielectric constant was measured by both the Von-Hippel method and by directly



measuring the guide wavelength in a slotted line completely filled with the sample material. Both methods of measurement gave an  $\epsilon_r$  which was within approximately  $\pm 1$  percent of the published value of 2.25. This is within the accuracy of the measurements; thus, one can justifiably take the dielectric constant as 2.25 within this accuracy.

The polyethylene sleeve was "heat fitted" on the cylinder so as to make a snug fit, and it is estimated that the accuracy of concentricity of the outer surface and inner surface of the dielectric coating was within  $\pm 0.010$  inch. The slip fitting of the dielectric sleeve on the metal cylinder is depicted in the photograph of figure 14.

The measurements of admittance were made in the conventional manner as with the condition of no coating. To realize the short circuit condition and to avoid the necessity of removing the dielectric sleeve and then replacing it at each frequency used, the short was first placed on the non-coated cylinder at each of the frequencies to be used and the frequency setting was accurately determined by means of a frequency meter accurate to within  $\pm 2\frac{1}{2}$  mc (Hewlett-Packard Model X532B). These exact frequencies were then reused with the short removed and the dielectric sleeve in position.

Plots of  $g_{in}$  and  $b_{in}$  are shown in figures 15 and 16, respectively.

Measurements were then repeated for four different circumferential positions of the dielectric sleeve at each of several frequencies, as shown in table I and figures 15 and 16. The dielectric positions were separated by increments of  $90^\circ$  and designated by positions A, B, C, and D as defined in table I. It is seen from figures 15 and 16 that the resultant admittance differs for each position of the dielectric even though the frequency was held constant. This can be attributed to one or both of the following

reasons: for each position the "effective dielectric constant" of the coating differs due to the approximately  $\pm 1$  percent deviation in the circumferential variation of dielectric constant which exists; for each position the effective thickness of the dielectric coating differs due to the inner and outer radial variation of approximately  $\pm 0.010$  inch. In either case, such changes influence the mean electrical circumferential length of the coating,  $\bar{C}$ , here defined by:

$$\bar{C} = \frac{2\pi\bar{a}}{\lambda_v} \bar{N} = \frac{C}{2}(W + 1)\bar{N} \quad (17)$$

where  $\bar{a}$  is the mean radius ( $\bar{a} = \frac{a+b}{2}$ ) and  $\bar{N}$  is the mean refractive index. It is seen that the change in  $\bar{C}$  due to changes in  $\bar{a}$  (i.e.,  $W$ ) and/or  $\bar{N}$  is

$$\Delta\bar{C} = \frac{C}{2}(W + 1)\Delta\bar{N} + \bar{N} \Delta W \quad (18)$$

which since  $W \approx 1$  and  $\Delta W = \Delta T/a$  is

$$\Delta\bar{C} = \frac{C}{2} 2 \Delta\bar{N} + \bar{N} \frac{\Delta T}{a} \quad (19)$$

It is recognized that the first term contributing to  $\Delta\bar{C}$  is the change in circumferential electrical length due to the change in the refractive index of the coating whereas the second is due to the change in thickness of the coating. Now, here upper limits of  $\Delta\bar{N}$  and  $\Delta T/a$  are approximately  $\Delta\bar{N}_{\max} = \pm 0.02$  and  $\Delta T/a = \pm 0.004$  so that  $\Delta\bar{C} \approx C (0.024)$ ,  $\Delta\bar{C}_{\max} \approx 0.024C_{\max}$ . For the cylinder used at X-band,  $C_{\max} \approx 45$ , therefore, the maximum change in  $C$  can be  $\Delta C_{\max} \approx 1.0$ ; i.e., the mean circumferential electrical length of the coating can approach the order of a wavelength in the coating material. Intuitively, one would expect that such a

change could very well lead to a large change in input admittance. It is seen that the major contribution to  $\Delta \bar{C}$  is from  $\Delta \bar{N}$ . Thus, for large cylinders (large  $C$ 's) small changes in the refractive index may be expected to account for the observed changes in admittance.

To make meaningful measurements of the input admittance and to compare them with computed results, it follows that stricter tolerances on the refractive index and coating thickness will be necessary if one uses electrically large cylinders. These tolerances will be correspondingly reduced (as seen from eq. (19)) for smaller cylinders. It would seem then that for an initial test of theory it may be more appropriate to use smaller cylinders.

The radiation patterns also seemed to be sensitive to small changes in the electrical parameters. The measured equatorial plane patterns are shown in figures 17(a) to 17(f) along with the corresponding computed patterns (using expression 335 of Wait<sup>2</sup>). It is seen that the agreement between theory and experiment in the forward direction is quite satisfactory; however, at the higher frequencies ( $k = 0.80, 0.85$ , and  $0.90$ ) the radiation level measured in the rear was considerably higher than that predicted, although for the lower frequencies ( $k = 0.65, 0.70$ , and  $0.75$ ) agreement at the rear is still satisfactory. The poor agreement in the rear direction may also be attributed to the critical dependence on the parameters of  $N$  and  $W$ .

#### ADMITTANCE OF A COATED AXIAL SLOT

From the work of Wait<sup>2</sup> the pertinent fields established in region 1 ( $a \leq \rho \leq b$ ) and region 2 ( $b \leq \rho \leq \infty$ ) of figure II-1 are given by (336), (337), (339), (340), and (342), (343), (345), (346) of Wait, respectively.

For the sake of brevity, these expressions will not be rewritten here, but it is noted that the following difference in notation is used:

Wait's notation	Notation of this report
$\mu$	$\mu_v$
$u_o$	$u_v$
$k_o$	$\beta_v$

Furthermore, it is noted here that in table I of Wait<sup>2</sup> (p. 128) that the coefficient  $b_{m1}$  should be multiplied by  $u$ , and the coefficient  $a_{m5}$  is lacking a minus sign.

Here again the tangential electric fields on the cylindrical surface  $\rho = a$  are assumed to be

$$E_\phi(a, \phi, z) = \begin{cases} 0 & \text{off slot} \\ E_o \cos\left(\frac{\pi z}{l}\right) & \text{on slot} \end{cases} \quad (20a)$$

$$E_z(a, \phi, z) = 0 \quad (20b)$$

From equation (20a) it follows that the transform of  $E_\phi$  is

$$\bar{E}_{\phi m}(h, a) = \frac{1}{(2\pi)^2} \int_{-\pi}^{\pi} \int_{-\infty}^{\infty} E_\phi(a, \phi, z) e^{jhz} e^{jm\phi} dz d\phi \frac{-\sqrt{a_m} V_o \cos\left(\frac{h l}{2}\right)}{2\pi\left(\frac{a}{l}\right)(h^2 l^2 - \pi^2)} \quad (21)$$

and from (339) of Wait the transform of  $H_z$  is

$$\bar{H}_{zm}(h, a) = u^2 \left[ b_m H_m^{(2)}(ua) + B_m J_m(ua) \right] \quad (22)$$

From Parseval's theorem the external (radiation) admittance is

$$Y_c = \frac{2P_c}{|V_o|^2} = \frac{1}{2}(2\pi)^2 \sum_{m=-\infty}^{m=+\infty} \int_{-\infty}^{\infty} \bar{E}_{\phi m}(h,a) \bar{H}_{zm}(h,a) dh \quad (23)$$

Using the six tangential boundary conditions (continuity of  $E_{\phi}$ ,  $E_z$ ,  $H_{\phi}$ ,  $H_z$  at  $\rho = b$ , and continuity of  $E_{\phi}$  and  $E_z$  at  $\rho = a$ ) and determinants gives expressions for  $B_m$ ,  $b_m$ , and  $D_m$ , respectively, where  $D_m$  is the determinant formed by the coefficients  $a_{mp}$ , etc., in table I, p. 128, of Wait.

Explicitly solving for  $B_m$ ,  $b_m$ , and  $D_m$  and substituting the expressions into equation (23) then gives

$$Y_c = \frac{a}{\alpha \mu \sqrt{\frac{a}{b}}} \sum_{m=-\infty}^{m=+\infty} J_{am} \int_{-\infty}^{\infty} \frac{u \cos^2\left(\frac{h}{2}\right) \left\{ \beta_v^2 u^2 u_v^2 \left[ H_m^{(2)}(u_v b) - u_{vm} H_m^{(2)'}(u_v b) \right] \left[ u_v H_m^{(2)}(u_v b) - u_{vm} H_m^{(2)'}(u_v b) \right] - \left( \frac{u_h}{b} \right)^2 (u^2 - u_v^2)^2 V_m^2 \left[ H_m^{(2)}(u_v b) \right]^2 \right\}}{(h^2 - \pi^2)^2 \left\{ \beta_v^2 u^2 u_v^2 \left[ H_m^{(2)}(u_v b) - u_{vm} H_m^{(2)'}(u_v b) \right] \left[ u_v H_m^{(2)}(u_v b) - u_{vm} H_m^{(2)'}(u_v b) \right] - \left( \frac{u_h}{b} \right)^2 (u^2 - u_v^2)^2 V_m^2 \left[ H_m^{(2)}(u_v b) \right]^2 \right\}} dh \quad (24)$$

where:

$$U_m = J_m(ua) H_m^{(2)'}(ub) - J_m'(ub) H_m^{(2)}(ua) \quad (25a)$$

$$V_m = J_m(ua) H_m^{(2)}(ub) - J_m(ub) H_m^{(2)}(ua) \quad (25b)$$

$$L_m = J_m(ub) H_m^{(2)'}(ua) - J_m'(ua) H_m^{(2)}(ub) \quad (25c)$$

$$T_m = J_m'(ub) H_m^{(2)'}(ua) - J_m'(ua) H_m^{(2)'}(ub) \quad (25d)$$

As a partial check on equation (24), consideration of the special case of no coating ( $b = a$ ) or an air coating ( $N = 1$ ) each cause equation (24) to reduce to equation (15a) and (15b) as should be

Rationalization and normalization of equation (24) then gives

$$g_c|_{N \geq 1} = \frac{32}{(\beta_{vl})^4 \left(\frac{a}{l}\right)^2 \pi^3} \sum_{m=0}^{\infty} \frac{a_m}{(1 + \delta_{0m})} \int_0^1 \frac{\left\{ (N^2 - y^2)(1 - y^2) \cos^2\left(\frac{\beta_{vl} y}{2}\right) \left[ (N^2 - y^2)(CW)^2 \left| N^2 \sqrt{1 - y^2} \bar{U}_{mH_m}^{(2)}(X) \right. \right. \right.}{\left[ y^2 - \frac{\pi^2}{(\beta_{vl})^2} \right]^2 \left\{ (CW)^2 (N^2 - y^2)^2 (1 - y^2) \left[ N^2 \sqrt{1 - y^2} \bar{U}_{mH_m}^{(2)}(X) \right. \right. \right.} \\ \left. \left. \left. - \sqrt{N^2 - y^2} \bar{V}_{mH_m}^{(2)'}(X) \right\}^2 + (my)^2 (N^2 - 1)^2 \bar{V}_m^2 \left| H_m^{(2)}(X) \right|^2 \right\}}{dy} \quad (26)$$

where  $X \equiv CW \sqrt{1 - y^2}$ ,

$$\left. \begin{aligned} \bar{L}_m &= \left[ J_m(X) Y_m' \left( \frac{X}{W} \right) - J_m' \left( \frac{X}{W} \right) Y_m(X) \right] \\ \bar{T}_m &= \left[ J_m'(X) Y_m' \left( \frac{X}{W} \right) - J_m' \left( \frac{X}{W} \right) Y_m'(X) \right] \\ \bar{U}_m &= \left[ J_m \left( \frac{X}{W} \right) Y_m'(X) - J_m'(X) Y_m \left( \frac{X}{W} \right) \right] \\ \bar{V}_m &= \left[ J_m \left( \frac{X}{W} \right) Y_m(X) - J_m(X) Y_m \left( \frac{X}{W} \right) \right] \\ \bar{L}_m &= -j \bar{L}_m \\ \bar{T}_m &= -j \bar{T}_m \\ \bar{U}_m &= -j \bar{U}_m \\ \bar{V}_m &= -j \bar{V}_m \end{aligned} \right\} \quad (27)$$

It is important to note that the above expression was also derived independently by integrating the Poynting vector over a spherical surface of radius  $r$  in the far field. As a partial check on equations (27) the case

of no coating ( $b = a$ , i.e.,  $W = 1$ ) or an air coating ( $W = 1$ ) both reduce equations (27) to equation (15a) as should be.

It is noted that the above reduction of  $y_c$  shows that only the integration from  $0 \leq y \leq 1$  contributes to the conductance (which may be anticipated if one considers that the conductance can also be obtained using Poynting's vector and the radiation fields).

However, the expression for  $b_c$  will be of the form

$$b_c|_{N \geq 1} = \int_0^1 + \int_1^N + \int_N^\infty \quad (28)$$

for the general case of an arbitrary homogeneous coating. As yet the explicit form for the integrands of equation (28) has not been obtained.

For the special case of a plasma coating at plasma resonance (one for which  $\omega = \omega_p$  and  $\nu = 0$ ) the refractive index is identically zero, i.e.,  $N = 0$ . For this condition, it has been shown that the equatorial plane radiation field is independent of  $\phi$  and that, therefore, the only term contributing to the fields in the summation over  $m$  is the  $m = 0$  term. This must also hold for the near fields and the fields over the plasma cylinder else no omnidirectionality would be possible. Thus for  $N = 0$ , only the  $m = 0$  mode of equation (25) need be retained (this can also be shown rigorously). In this case, only the zero order and first order Bessel, Hankel, and modified Bessel functions are involved. As such, the programing of the expression for  $y_c|_{N=0}$  should present no special problem.

An attempt was made to program a modified form of equation (27) in order to compute the conductance of the axial slot on the 13-inch-diameter coated cylinder. However, the results seemed to be in error by at least

6 percent. Possible errors in this computation are still being investigated by examining a plot of the integrand of equations (27).

#### THE CYLINDRICAL GAP ANTENNA

The antenna under discussion, shown in figures 18, 19, and 20, is essentially a cylindrical geometry version of a spherical slot antenna described by Musiake and Webster<sup>7</sup>. Such an antenna has interesting features that make it extremely useful as a diagnostic tool for reentry plasma sheaths. To name a few:

1. Its cylindrical structure with no protruding part allows it to be an integral part of the reentry vehicle.
2. The feed system consisting of the inner conductor of a coaxial cable across a gap much smaller than a wavelength supports a uniform current; as a result, solutions are possible without assuming an aperture field distribution.
3. In spite of such a narrow gap, the antenna is an excellent radiator when its circumference is approximately equal to 2 wavelengths. At VHF frequencies, the physical size of the antenna is compatible with the size of many small reentry vehicles.
4. An additional feature of the narrow gap is to rule out the existence of axial magnetic fields at the aperture and inside the gap. Consequently, only azimuthal  $E_{zm}$  modes are excited and this field distribution is maintained even in the presence of radially nonhomogeneous plasmas.
5. The antenna is a resonant structure whose radiation and impedance properties are determined only by one significant azimuthal mode. From the number of lobes in the radiation pattern, it is possible to determine the significant modal impedance.



6. Finally, this is an antenna which is amenable to simple mathematical analysis, permitting accurate prediction of both far and near field performance.

In this paper the antenna input impedance both with and without plasma coating is discussed. Experimental checks are only given for no coating, and are correlated to the radiation patterns.

#### INPUT IMPEDANCE WITH NO PLASMA COATING

Consider the cylindrical gap antenna depicted in figure 18. The gap width  $d$  is narrow compared to the free-space wavelength  $\lambda_0$  ( $d \ll \lambda_0$ ) and is formed by a radial waveguide short-circuited at its center by a spacer of radius  $\rho = \rho_0$ . The gap is fed by a coaxial line located at the rim of the guide at  $\rho = a$ . The coax center conductor makes electrical contact with the guide top plate and its outer conductor is shorted out against the bottom plate. Because the gap width is small, with respect to the wavelength, the current along the coax inner conductor across the gap can be taken to be constant and equal to  $I$ . If the voltage in the coax is  $V_c$ , the antenna input impedance presented by the gap to the coax is

$$Z_{in} = -\frac{V_c}{I} \quad (29)$$

This is not merely a definition but also a measurable quantity related to the reflection coefficient  $\Gamma$  in the coax via its characteristic impedance  $Z_c$ ,

$$Z_{in} = Z_c \frac{1 + \Gamma}{1 - \Gamma} \quad (30)$$

In order to calculate  $Z_{in}$ , refer to figure 21 which shows the feed region grossly enlarged. The voltages  $V_c$  and  $V_a$  in the coax and in the aperture, respectively, are related by Maxwell's equations to the magnetic flux

enclosed by the line integral of the electric field yielding these voltages, that is,

$$V_a - V_c = -\frac{\partial}{\partial t} \iint \vec{B} \cdot d\vec{S} \quad (31)$$

for a perfectly conducting wire. The integration is over the surface defined by the loop boundary just described. The right-hand side of equation (32) is the inductive reactance of the loop,  $i\omega_0 L_l$  times the total current  $I$  flowing in the wires and spreading through the radial guide plates. Equation (29) can thus be rewritten after dividing by  $I$

$$-\frac{V_c}{I} = -\frac{V_a}{I} + i\omega_0 L_l \quad (32)$$

$\frac{-V_c}{I}$  is immediately recognized as the input impedance  $Z_{in}$  being sought. The ratio  $\frac{-V_a}{I}$  has the dimensions of an impedance and is defined as the antenna aperture impedance. It will be shown that the aperture impedance is not in general directly measurable, but in some cases it can be calculated from a knowledge of the fields in the aperture. The quantity  $i\omega_0 L_l$  can be considered to be solely due to the reactance of the loop.

Equation (32) may now be expressed as follows\*

$$Z_{in} = (Z_a + Z_{af}) + (Z_{fa} + Z_f) \quad (33)$$

where the first term in parenthesis is equal to  $\frac{-V_a}{I}$  and the second to  $i\omega_0 L_l$ . Each parenthesis consists of two parts, the self-impedances  $Z_a$ ,  $Z_f$ , and the mutual  $Z_{af} = Z_{fa}$ . (The  $f$  and  $a$  subscript denote, respectively, feed and aperture impedances.) The two impedances, aperture and

---

\*Dr. George I. Cohn made the analysis described by equations (33) to (38).

feed, can sometimes be calculated and/or measured independently of each other if the interaction caused by the mutual impedances is negligible. This is the case if the fields can be divided on a spatial basis into subvolumes such that the fields in any one subvolume can be attributed only to sources not producing fields in any other subvolume. Thus, if

$$|Z_{af}| \ll |Z_a| \quad (34a)$$

or

$$|Z_{af}| \ll |Z_f| \quad (34b)$$

then  $Z_a = \frac{-V_a}{I}$  is directly calculable from the fields in the gap which are obtained by solving the electromagnetic boundary value problem.  $Z_f$  is the wire inductive reactance in the absence of the gap.

The flux common to two subvolumes is always less than the self-linking flux; therefore,

$$|Z_{af}| \leq |Z_a| \quad (35a)$$

or

$$|Z_{af}| \leq |Z_f|$$

One way to insure separability of impedances as given by equation (33) is to demand

$$|Z_a| \ll |Z_f| \quad (36a)$$

or

$$|Z_f| \ll |Z_a| \quad (36b)$$

that is, either the wire inductive reactance is much smaller than the aperture impedance or vice versa. It will be shown that the feed wire inductive reactance can be made to fulfill the inequality equation (36b) for the gap antenna in question and vanishes as the gap goes to zero. The feed

impedance  $Z_f$  and the aperture impedance  $Z_a$  (in the absence of coupling between them) will now be calculated, keeping in mind that as long as equation (36b) is satisfied, the antenna input impedance  $Z_{in}$  is the sum of these two contributions.

An upper bound on the feed wire inductive reactance is established by calculating the inductance of a coaxial line of length  $d$  with inner and outer radii  $r_1$  and  $r_2$ . Using the geometrical approximation, it is easily shown that

$$Z_f = 377 \frac{d}{\lambda_0} \ln \frac{r_2}{r_1} \Omega \quad (37)$$

If  $\frac{d}{\lambda_0} \sim \frac{1}{30}$  and  $\frac{r_2}{r_1} \sim 10$ .

$$|Z_f| \sim 30\Omega \quad (38)$$

Since the antenna is to have an input impedance of  $50\Omega$  resistive in order to match the coax characteristic impedance, equation (36) is not fulfilled and the input impedance is not separable into feed and aperture. Changing the outer to inner coax radii ratio in equation (37) is not as effective as reducing the gap width since the logarithm varies slowly with the ratio in question. However, if the gap width is reduced by  $1/2$  or  $1/3$  corresponding to  $d/\lambda_0$  of the order of  $1/60$  to  $1/100$ , equation (36) is fulfilled and the impedance is separable.

The solution of the electromagnetic fields subject to the boundary conditions yields the aperture admittance,  $Y_m = \frac{I}{-V_m}$  for each peripheral mode  $m$ , where  $V_m = E_{zm} d$ , is the voltage across the gap for the  $m$ th mode as shown in figure 22. The total aperture impedance is in turn related to  $Y_m$  by

$$Z_a = \sum_m \frac{1}{Y_m} = \sum_m \frac{1}{G_m + i(B_m^i + B_m^e)} \quad (39)$$

where  $B_m^i$  is the susceptance presented at the feed by the interior region, and  $G_m$  and  $B_m^e$  is the admittance contributed by the exterior region. For a narrow gap, with uniform feed current, the resultant modal admittance  $Y_m$  normalized with respect to the wave impedance in the exterior space  $Y_0$  ( $(120\Omega)^{-1}$  for free space) has been found to be

$$\begin{aligned} y_m &= g_m + i(b_m^e + b_m^i) \\ g_m &= \frac{1}{\pi} \left\{ \int_0^1 \frac{\sin^2 c^2 \frac{x d_0}{2}}{[H_m(2)(a_0 \sqrt{1-x^2})]^2} \frac{dx}{1-x^2} + \left(\frac{a_0}{d_0}\right)^2 \int_0^1 \frac{\sin^2 c^2 \frac{x d_0}{2}}{[H_m(2)(a_0 \sqrt{1-x^2})]^2} \frac{x^2}{(1-x^2)^2} dx \right\} \\ b_m^e &= 12a_0 \left\{ \int_0^1 \frac{J_m(a_0 \sqrt{1-x^2}) J_m'(a_0 \sqrt{1-x^2}) + Y_m(a_0 \sqrt{1-x^2}) Y_m'(a_0 \sqrt{1-x^2})}{[H_m(2)(a_0 \sqrt{1-x^2})]^2} \sin^2 c^2 \frac{x d_0}{2} \frac{dx}{\sqrt{1-x^2}} - \int_1^\infty \frac{Y_m'(a_0 \sqrt{x^2-1})}{K_m(a_0 \sqrt{x^2-1})} \sin^2 c^2 \frac{x d_0}{2} \frac{dx}{\sqrt{x^2-1}} \right. \\ &\quad \left. - \left(\frac{a_0}{d_0}\right)^2 \left[ \int_0^1 \frac{J_m(a_0 \sqrt{1-x^2}) J_m'(a_0 \sqrt{1-x^2}) + Y_m(a_0 \sqrt{1-x^2}) Y_m'(a_0 \sqrt{1-x^2})}{[H_m(2)(a_0 \sqrt{1-x^2})]^2} \sin^2 c^2 \frac{x d_0}{2} \frac{x^2 dx}{(1-x^2)^{3/2}} - \int_1^\infty \frac{Y_m'(a_0 \sqrt{x^2-1})}{K_m(a_0 \sqrt{x^2-1})} \sin^2 c^2 \frac{x d_0}{2} \frac{x^2 dx}{(x^2-1)^{3/2}} \right] \right\} \\ b_m^i &= -i \frac{2\pi a_0}{d_0} \left[ \frac{J_m'(a_0) Y_m(r_0) - J_m(r_0) Y_m'(a_0)}{[J_m(a_0) Y_m(r_0) - J_m(r_0) Y_m'(a_0)]} \right] \quad \sin c^2 \frac{x d_0}{2} = \frac{\sin(\frac{x d_0}{2})}{(\frac{x d_0}{2})} \end{aligned} \quad (40)$$

$x$ ,  $a_0$ ,  $d_0$ ,  $r_0$  being respectively normalized: wave number  $k/k_0$ , cylinder radius  $k_0 a$ , gap width  $k_0 d$ , spacer radius  $k_0 \rho_0$ .  $Y_m$  was derived by calculating the fields in both regions, matching them at the boundaries between antenna and exterior region taking into account the discontinuity in current.

For each mode  $m$ , there exists a current sheath  $J_{zm}$  around the gap periphery which is independent of  $z$  (fig. 22). The electric field across the gap resulting from this current density is also independent of  $z$  at the interface. It follows that the locally induced magnetic field at the interface does not vary along the gap width. Pursuing this reasoning

reasoning further, only a  $z$ -dependent  $H_\phi$  could produce an  $E_\rho$  component and this one in turn would produce an  $H_z$ . One therefore concludes that, in the absence of  $z$ -dependent field components, no  $H_z$  component is generated at the gap interface.

#### EVALUATION OF APERTURE IMPEDANCE $Z_a$

Equation (40) for  $g_m$ ,  $b_m^e$ , and  $b_m^i$  was used to calculate the various modal impedances for a frequency scaled up model of the cylindrical gap antenna under study. The model shown in figures 19 and 20 was designed to operate around 1090 mc with the following parameters:

Gap width,  $d = \frac{7}{32}$  inch,  $d_0 = 0.156$

Spacer radius,  $\rho_0 = 1$  inch

Gap radius,  $a = 3$  inches,  $a_0 = 2.13$

Operating wavelength,  $\lambda_0 = 8.81$  inches

Graphs showing pertinent calculations of  $g_0$ ,  $b_0^e$ , and  $b_1^m$  are shown in figures 23, 24, and 25. The calculated normalized conductance and susceptance for the above parameters as well as the unnormalized corresponding impedances are shown in table II for mode numbers ranging from  $m = 0$  to  $m = 9$ . The important feature of these results is the fact that for an antenna circumference approximately two wavelengths, the first order mode ( $m = 1$ ) contributes most significantly to the impedance. The modes below ( $m = 0$ ) have a reactance that tends to cancel the reactance of the modes above it ( $m \geq 2$ ). In essence, for each value of  $a_0$  the antenna is a resonant structure, with one contributing mode. (For  $a_0 \sim 1$  it can be shown that  $Z_0$  is the resonant impedance.) The resonant mode determines both the impedance as well as the radiation characteristics. For the

specific choice of parameters above  $a_0 = 2.13$ , the measured radiation pattern shown in figure 26 exhibits the two lobes that one would expect from the  $m = 1$  cosinusoidal aperture distribution of figure 22. Therefore, the size of the antenna establishes only one specific mode as the contributing one and this mode in turn determines uniquely both the input impedance and the radiation fields.

#### APERTURE IMPEDANCE IN THE PRESENCE OF A NONHOMOGENEOUS PLASMA

The plasma model under consideration is represented by a radially varying dielectric uniform, in the  $\phi$ - and  $z$ -direction.

The approach followed is the one developed by C. T. Swift<sup>8</sup>. The plasma is subdivided in  $n$ -concentric cylindrical sheaths. Each sheath is taken to have a uniform plasma and collision frequency equal to its average through the sheath.

The fields in the radial waveguide are matched at the interface to those in the first sheath. The field transforms in each sheath are no longer forward traveling waves expressed in terms of Hankel functions. They are standing waves consisting of the linear superposition of Hankel and Bessel functions. The fields in Region I and the first sheath of Region II are

##### Region I

$$\left. \begin{aligned} E_{zm}^I &= \frac{V_m}{d} \\ H_{\phi m}^I &= -iY_0 \frac{V_m}{d} \frac{F_m'(k_0 \rho)}{F_m(k_0 \rho)} \\ H_{\rho m}^I &= -iY_0 \frac{m}{k\rho} \frac{V_m}{d} \end{aligned} \right\} \quad (41)$$

Region II (1st layer)

$$\left. \begin{aligned} \bar{E}_{zm}^{II1} &= u_1 \bar{\mathcal{J}}_m^1 \\ \bar{H}_{\phi m}^{II1} &= -iY_{01}k_{01}u_1 \bar{\mathcal{J}}_m^{1'} - \frac{km}{\rho} \bar{\mathcal{J}}_m^1 \\ \bar{H}_{\rho m}^{II1} &= -Y_{01}k_{01} \frac{m}{\rho} \bar{\mathcal{J}}_m^1 + iku_1 \bar{\mathcal{J}}_m^1 \end{aligned} \right\} \quad (42)$$

$$\left. \begin{aligned} \bar{H}_{zm}^{II1} &= u_1 \bar{\mathcal{J}}_m^1 \\ \bar{E}_{\phi m}^{II1} &= -\frac{km}{\rho} \bar{\mathcal{J}}_m^1 + iZ_{01}k_{01}u_1 \bar{\mathcal{J}}_m^{1'} \\ \bar{E}_{\rho m}^{II1} &= iku_1 \bar{\mathcal{J}}_m^{1'} + Z_{01}k_{01} \frac{m}{\rho} \bar{\mathcal{J}}_m^1 \end{aligned} \right\} \quad (43)$$

The foregoing expressions for Region I were obtained after making the substitution

$$u_0^2 = k_0^2$$

$$u_0^2 a_{m0} F_{m0}(u_0 \rho) = \frac{V_m}{d}$$

In Region II, forward traveling waves are replaced by the standing waves, i.e.,

$$\left. \begin{aligned} c_m(k) H_m^{(2)}(u\rho) &\rightarrow \bar{\mathcal{J}}_m^1(k_1 u\rho) = a_m^1(k) J_m(u_1 \rho) + A_m^1(k) H_m^{(2)}(u_1 \rho) \\ d_m(k) H_m^{(2)}(u\rho) &\rightarrow \bar{\mathcal{J}}_m^1(k_1 u\rho) = b_m^1(k) J_m(u_1 \rho) + B_m^1(k) H_m^{(2)}(u_1 \rho) \end{aligned} \right\} \quad (44)$$

$\bar{\mathcal{J}}_m^{1'}$  and  $\bar{\mathcal{J}}_m^1$  are derivatives with respect to the argument  $(u_1 \rho)$ .



The modal aperture admittance  $Y_m$  is now expressed in terms of these unknown coefficients by demanding that

$$H_m^{II} - H_m^I = \frac{I}{2\pi a} \quad 0 \leq z \leq d \quad (45)$$

Using the expressions (41) and (42), it follows that

$$\begin{aligned} -iY_0 k_{01} \int_{-\infty}^{\infty} a_m^1 J_m'(u_1 a) + A_m^1 H_m^{(2)'}(u_1 a) u_1 e^{ikz} dk - \frac{m}{a} \int_{-\infty}^{\infty} b_m^1 J_m(u_1 a) \\ + B_m^1 H_m^{(2)}(u_1 a) e^{ikz} k dk + iY_0 \frac{F_m'(k_0 a)}{F_m(k_0 a)} \frac{V_m}{d} = \frac{I}{2\pi a} \quad 0 \leq z \leq d \end{aligned} \quad (46)$$

In order to eliminate the dependence on  $z$ , both sides of equation (46) are integrated from 0 to  $d$ . And, use of the relation

$$\frac{1}{d} \int_0^d e^{ikz} dz = C_0(k)$$

results in

$$\begin{aligned} -iY_0 k_{01} \int_{-\infty}^{\infty} \left[ a_m^1 J_m^1(u_1 a) + A_m^1 H_m^{(2)'}(u_1 a) \right] u_1 C_0(k) dk - \frac{m}{a} \int_{-\infty}^{\infty} \left[ b_m^1 J_m(u_1 a) \right. \\ \left. + B_m^1 H_m^{(2)}(u_1 a) \right] k C_0(k) dk + iY_0 \frac{F_m'(k_0 a)}{F_m(k_0 a)} \frac{V_m}{d} = \frac{I}{2\pi a} \end{aligned} \quad (47)$$

In order to find  $Y_m$  the four coefficients  $a_m^1$ ,  $A_m^1$ ,  $b_m^1$ , and  $B_m^1$  must be expressed in terms of  $V_m$ . This is done as follows.

As shown by Swift\* a Transfer Function can be developed which relates via a  $4 \times 4$  matrix the unknown coefficients,  $a_m^1$ ,  $A_m^1$ ,  $b_m^1$ , and  $B_m^1$  in the first sheath to the free-space coefficients  $c_m, d_m$  beyond the last sheath. The transfer function depends only on the values of  $J_m(u_1 \rho_1)$  and  $H_m(u_1 \rho_1)$  at each sheath and the corresponding plasma parameters. The matrix coefficients are labeled  $C_{jk}$ . Their values are given in the cited reference. The following relation holds among these coefficients

$$\begin{bmatrix} a_m^1 \\ A_m^1 \\ b_m^1 \\ B_m^1 \end{bmatrix} = \begin{bmatrix} C_{11} & C_{12} & C_{13} & C_{14} \\ C_{21} & C_{22} & C_{23} & C_{24} \\ C_{31} & C_{32} & C_{33} & C_{34} \\ C_{41} & C_{42} & C_{43} & C_{44} \end{bmatrix} \begin{bmatrix} 0 \\ c_m \\ 0 \\ d_m \end{bmatrix} \quad (48)$$

The preceding equations reduce the number of unknowns from 4 to 2. Application of the two tangential boundary conditions at the antenna surface, i.e.,

$$\left. \begin{aligned} \bar{E}_{zm} &= \frac{V_m}{2\pi} C_o^*(k) \\ \bar{E}_{\phi m} &= 0 \end{aligned} \right\} \quad (49)$$

---

\*The field expressions are different from Swift because the factor  $\frac{1}{i\omega\mu_0\epsilon_1}$  is absorbed in the coefficients  $a_m^1(k)$ ,  $A_m^1(k)$ ,  $b_m^1(k)$ , and  $B_m^1(k)$ . Furthermore, the fields are constructed from  $e^{im\phi}e^{ikz}$  while Swift uses negative exponents. The above expressions can be converted to Swift's by dividing all field transforms by  $\omega\mu_0\epsilon_1$  and changing  $m$  and  $k$  into  $-m$  and  $-k$ .

allows the unknown coefficient  $c_m$  and  $d_m$  and, consequently,  $a_m^1$ ,  $A_m^1$ ,  $b_m^1$ , and  $B_m^1$  to be expressed in terms of  $V_m$ . The derivation now follows.

Equation (48) can be written as

$$\left. \begin{aligned} a_m^1 &= C_{12}c_m + C_{14}d_m \\ A_m^1 &= C_{22}c_m + C_{24}d_m \\ b_m^1 &= C_{32}c_m + C_{34}d_m \\ B_m^1 &= C_{42}c_m + C_{44}d_m \end{aligned} \right\} \quad (50)$$

Therefore, from equations (47), (49), and (43), after using equation (50), it follows that

$$\left. \begin{aligned} \left\{ C_{12}J_m + C_{22}H_m^{(2)} \right\} c_m + \left\{ C_{14}J_m + C_{24}H_m^{(2)} \right\} d_m &= \frac{V_m}{2\pi u_1^2} C_o^*(k) \\ \left\{ C_{32}J_m' + C_{42}H_m^{(2)} + iY_{01} \frac{m}{u_1 a} \frac{k}{k_{01}} [C_{12}J_m + C_{22}H_m^{(2)}] \right\} c_m + \left\{ C_{34}J_m' + C_{44}H_m^{(2)} + iY_{01} \frac{m}{u_1 a} \frac{k}{k_{01}} [C_{14}J_m + C_{24}H_m^{(2)}] \right\} d_m &= 0 \end{aligned} \right\} \quad (51)$$

Solving for  $c_m$  and  $d_m$  in terms of  $V_m$  and expressing  $a_m^1$ ,  $A_m^1$ ,  $b_m^1$ , and  $B_m^1$  in terms of  $V_m$  via equation (49) and substituting into equation (41) results in the following expression for the modal antenna aperture admittance covered with plasma.

$$\begin{aligned} \frac{Y_m}{iY_{01}} &= k_{01}a \int_{-\infty}^{\infty} (C_{12}C_{34} - C_{14}C_{32})(J_m')^2 + (C_{22}C_{44} - C_{24}C_{42})(H_m^{(2)})'^2 + (C_{12}C_{44} - C_{14}C_{42} + C_{22}C_{34} - C_{24}C_{32})J_m'H_m^{(2)} \frac{C_o^*C_o}{\Delta} \frac{dk}{u_1} \\ &- \frac{m^2}{k_{01}a} \int_{-\infty}^{\infty} (C_{12}C_{34} - C_{14}C_{32})(J_m)^2 + (C_{22}C_{44} - C_{24}C_{42})(H_m^{(2)})^2 + (C_{12}C_{44} - C_{14}C_{42} + C_{22}C_{34} - C_{24}C_{32})J_mH_m^{(2)} \frac{C_o^*C_o}{\Delta} \frac{k^2}{u_1^2} \frac{dk}{u_1} - \frac{2\pi a}{d} \frac{F_m'}{F_m} \end{aligned} \quad (52)$$

where  $\Delta$  the determinant of the  $4 \times 4$  matrix in equation (51) is given by:

$$\begin{aligned} \Delta = & (C_{12}C_{34} - C_{14}C_{32})J_m J_m' + (C_{12}C_{44} - C_{14}C_{42})J_m H_m(2)' \\ & + (C_{22}C_{34} - C_{24}C_{32})J_m' H_m(2) + (C_{22}C_{44} - C_{24}C_{42})H_m(2)H_m(2)' \end{aligned} \quad (53)$$

It is understood that the arguments of the cylindrical functions are  $u_1 a = \sqrt{(k_{01}^2 - k^2)}a$ . The quantity  $k_{01}$  is the wave number in the first plasma sheath adjacent to the antenna.

As a partial check on the validity of expression (52), the plasma is removed, in which case

$$C_{12} = C_{14} = C_{24} = C_{32} = C_{34} = C_{42} = 0$$

$$C_{22} = C_{44} = 1$$

$$k_{01} = k_0$$

$$u_1 = u$$

The admittance now reduces to

$$\frac{Y_m}{iY_{01}} = \left\{ k_0 a \int_{-\infty}^{\infty} \frac{H_m(2)'}{H_m(2)} C_0^* C_0 dk - \frac{m^2}{k_0 a} \int_{-\infty}^{\infty} \frac{H_m(2)}{H_m(2)'} C_0^* C_0 \frac{dk}{u} - \frac{2\pi a}{d} \frac{F_m'(k_0 a)}{F_m(k_0 a)} \right\} \quad (54)$$

where  $C_0^* C_0 = \sin c^2 \frac{kd}{2}$ .

Equation (54) is equivalent to equation (40) prior to breaking it into real and imaginary parts.

## CONCLUDING REMARKS

This investigation of slotted cylinders has led to the following conclusions:

(1) For the case of resonant coating ( $\omega = \omega_p$ ,  $\nu = 0$ ), the admittance approaches zero as the thickness of the coating increases. At intermediate thicknesses, the susceptance can change from a large capacitive to a small inductive value or to zero.

(2) For all practical purposes, the admittance of identical slots on cylinders and ground planes is equivalent if the circumference-to-wavelength ratio of the cylinder is greater than four and if the loss angle of the plasma lies between  $90^\circ$  and  $180^\circ$ , and the magnitude of  $N \gtrsim 1$ .

(3) For the reentry plasma distribution shown in figure 7, the admittance undergoes pronounced changes when the propagating frequency approaches the peak plasma frequency.

(4) The admittance of apertures on large coated cylinders ( $C \gtrsim 20$ ) seems to be sensitive to slight changes in the electrical and mechanical tolerances of the coating. As such, one is led to conclude that theoretical results will be difficult to realize experimentally unless electrically small cylinders are used ( $C \lesssim 10$ ).

(5) The resonant properties of the cylindrical gap antenna indicate that it may be useful for plasma diagnostics. The presence of plasma or any change of antenna parameters brings one azimuthal mode into prominence which determines both the shape of the radiation pattern and the value of the antenna input impedance. As the plasma varies in density, it would be expected that various modes would be successively excited; therefore, one could expect the pattern and the input impedance to change accordingly.

# APPENDIX I

## LIST OF SYMBOLS USED IN THE ANALYSIS OF THE AXIAL SLOT

a	radius of conducting cylinder
$a_m$	$\frac{\sin \frac{m\phi_0}{2}}{\frac{m\phi_0}{2}}$
B	susceptance
b	radial distance to air-plasma interface
C	circumference of cylinder in wavelengths = $\frac{2\pi a}{\lambda_v}$
E	electric field
$\bar{E}, \bar{\bar{E}}$	Fourier transforms of electric field
$E_0$	amplitude of electric field at aperture
$\vec{E}_0$	amplitude of incident $TE_{01}$ wave
G	conductance
H	magnetic field
$\bar{H}, \bar{\bar{H}}$	Fourier transforms of the magnetic field
h	axial mode number
k	length of slot in wavelengths = $l/\lambda_v$
l	length of slot
m	azimuthal mode number
N	index of refraction
P	power
p	$a/l$
S	Poynting vector
u	radial mode number
$V_0$	applied potential on slot

$$W = b/a$$

$w$  width of slot

$Y$  admittance

$Y_0$  admittance of free space

$Y_{01}$  waveguide admittance of  $TE_{01}$  mode

$\beta$  wave number

$\beta_{01}$  wave number for the  $TE_{01}$  waveguide mode

$\Gamma$  reflection coefficient

$\delta_m^n$  Kronecker delta =  $\begin{cases} 0 & m \neq n \\ 1 & m = n \end{cases}$

$\epsilon$  dielectric constant

$\epsilon_0$  permittivity of free space

$\epsilon_r$  real part of the dielectric constant

$\eta, \xi$  transverse components within a rectangular waveguide

$\lambda$  wavelength

$\lambda_{g01}$  guide wavelength

$\mu_0$  permeability of free space

$\nu$  electron collision frequency

$\rho, \phi, z$  cylindrical coordinates

$\phi_0$  angular width of slot

$\omega$  exciting frequency

$\omega_p$  plasma frequency

Subscripts:

$c$  external

$in$  input

$l$  per unit length

• R            plasma resonant  
v            vacuum  
 $\eta$             vector component along narrow dimension of waveguide  
 $\rho, \phi, z$        vector components along the three principal directions in  
             cylindrical coordinates



## APPENDIX II

### ADMITTANCE EXPRESSIONS FOR LONG SLOTS ON CYLINDERS

The pertinent fields in regions I and II of the structure shown in figure 1 are:

$$H_z^I(\rho, \phi) = \sum_{m=-\infty}^{\infty} A_m \left[ J_m(\beta \rho) + B_m H_m^{(2)}(\beta \rho) \right] e^{-jm\phi} \quad (\text{II-1})$$

$$H_z^{II}(\rho, \phi) = \sum_{m=-\infty}^{\infty} C_m H_m^{(2)}(\beta_v \rho) e^{-jm\phi} \quad (\text{II-2})$$

$$E_\phi^I(\rho, \phi) = \frac{j}{Y_0} \sqrt{\frac{\epsilon_0}{\epsilon}} \sum_{m=-\infty}^{\infty} A_m \left[ J_m'(\beta \rho) + B_m H_m^{(2)'}(\beta \rho) \right] e^{-jm\phi} \quad (\text{II-3})$$

$$E_\phi^{II}(\rho, \phi) = \frac{j}{Y_0} \sum_{m=-\infty}^{\infty} C_m H_m^{(2)'}(\beta_v \rho) e^{-jm\phi} \quad (\text{II-4})$$

where the prime denotes differentiation of the Bessel and Hankel functions with respect to the argument.

If it is assumed that the aperture field is of the form:

$$E_\phi(a, \phi) = \frac{V_0}{a} = \sum_{m=-\infty}^{\infty} \bar{E}_{m\phi}(a) e^{-jm\phi} = \frac{V_0}{2\pi a} \sum_{m=-\infty}^{\infty} \frac{\sin\left(\frac{m\phi_0}{2}\right)}{\left(\frac{m\phi_0}{2}\right)} e^{-jm\phi} \quad (\text{II-5})$$

then the boundary conditions at  $\rho = a$  and  $\rho = b$  give the following algebraic relationships

$$\frac{V_0}{2\pi a} \frac{\sin\left(\frac{m\phi_0}{2}\right)}{\left(\frac{m\phi_0}{2}\right)} = \frac{j}{NY_0} A_m \left[ J_m'(NC) + B_m H_m^{(2)'}(NC) \right] \quad (\text{II-6})$$

$$\frac{1}{N} A_m \left[ J_m'(NCW) + B_m H_m^{(2)'}(NCW) \right] = C_m H_m^{(2)'}(CW) \quad (II-7)$$

$$A_m \left[ J_m(NCW) + B_m H_m^{(2)}(NCW) \right] = C_m H_m^{(2)}(CW) \quad (II-8)$$

Solving the above equations for  $A_m$  and  $B_m$  gives:

$$A_m = -j\bar{E}_{m0}^{NY_0} \frac{NH_m^{(2)}(NCW)H_m^{(2)'}(CW) - H_m^{(2)}(CW)H_m^{(2)'}(NCW)}{H_m^{(2)}(CW)T_m - NH_m^{(2)'}(CW)L_m} \quad (II-9)$$

$$B_m = \frac{H_m^{(2)}(CW)J_m'(NCW) - NJ_m(NCW)H_m^{(2)'}(CW)}{NH_m^{(2)}(NCW)H_m^{(2)'}(CW) - H_m^{(2)}(CW)H_m^{(2)'}(NCW)} \quad (II-10)$$

where

$$\left. \begin{aligned} T_m &= J_m'(NCW)H_m^{(2)'}(NC) - J'(NC)H_m^{(2)'}(NCW) \\ L_m &= J_m(NCW)H_m^{(2)'}(NC) - J_m'(NC)H_m^{(2)}(NCW) \end{aligned} \right\} \quad (II-11)$$

Therefore:

$$\begin{aligned} \bar{H}_{mZ} &= A_m \left[ J_m(NC) + B_m H_m^{(2)}(NC) \right] \\ &= -j\bar{E}_{m0}^{NY_0} \left\{ \frac{NH_m^{(2)'}(CW)V_m - H_m^{(2)}(CW)U_m}{H_m^{(2)}(CW)T_m - NH_m^{(2)'}(CW)L_m} \right\} \end{aligned} \quad (II-12)$$

where

$$\left. \begin{aligned} U_m &= J_m(NC)H_m^{(2)'}(NCW) - J_m'(NCW)H_m^{(2)}(NC) \\ V_m &= J_m(NC)H_m^{(2)}(NCW) - J_m(NCW)H_m^{(2)}(NC) \end{aligned} \right\} \quad (II-13)$$

From Parseval's theorem, the external admittance per unit length is given

by

$$Y_{cl} = \frac{2P}{|V_0|^2} = 2\pi a \sum_{m=-\infty}^{\infty} \frac{\bar{E}_{m\phi}^* \bar{E}_{mz}}{|V_0|^2} \quad (\text{II-14})$$

And the substitution of equations (II-5) and (II-12) into equation (II-14) results in the following admittance expression

$$Y_{cl} = -\frac{j}{2\pi a} NY_0 \sum_{m=-\infty}^{\infty} \frac{\sin^2\left(\frac{m\phi_0}{2}\right)}{\left(\frac{m\phi_0}{2}\right)^2} \left\{ \frac{NH_m^{(2)'}(CW)V_m - H_m^{(2)}(CW)U_m}{H_m^{(2)}(CW)T_m - NH_m^{(2)'}(CW)L_m} \right\} \quad (\text{II-15})$$

For the case of no coating ( $\omega = 1$  or  $b = a$ ), equation (II-15) becomes:

$$Y_{cl} = -\frac{jY_0}{2\pi a} \sum_{m=-\infty}^{\infty} \frac{\sin^2\left(\frac{m\phi_0}{2}\right)}{\left(\frac{m\phi_0}{2}\right)^2} \frac{H_m^{(2)}(C)}{H_m^{(2)'}(C)} \quad (\text{II-16})$$

It has been shown<sup>1</sup> that at plasma resonance, the fields, hence the admittance, are indepent of the azimuthal coordinate,  $\phi$ . Therefore, only the  $m = 0$  mode is supported, and equation (II-15) reduces to

$$Y_{cl} = -\frac{jY_0}{2\pi a} \lim_{N \rightarrow 0} N \left\{ \frac{NH_0^{(2)'}(CW)V_0 - H_0^{(2)}(CW)U_0}{H_0^{(2)}(CW)T_0 - NH_0^{(2)'}(CW)L_0} \right\} \quad (\text{II-17})$$

In order to evaluate the above equation, the following expansions are necessary:

$$\left. \begin{aligned} J_0(x) &\approx 1 - \frac{x^2}{4} & J_0'(x) &\approx -\frac{x}{2} \\ Y_0(x) &\approx \frac{2}{\pi} \log x & Y_0'(x) &\approx \frac{2}{\pi x} \end{aligned} \right\} \quad (\text{II-18})$$

to give

$$\left. \begin{aligned} T_0 &\approx \frac{j}{\pi} \left[ W - \frac{1}{W} \right] & U_0 &\approx -j \frac{2}{\pi N C W} \\ L_0 &\approx -j \frac{2}{\pi N C} & V_0 &\approx -j \frac{2}{\pi} \log W \end{aligned} \right\} \quad (\text{II-19})$$

Therefore, for  $N = 0$  and  $W > 1$

$$Y_{CR} = -\frac{jY_0}{2\pi a} \frac{H_0^{(2)}(CW)}{\left[ W H_0^{(2)'}(CW) + \frac{CW}{2} H_0^{(2)}(CW) \left( W - \frac{1}{W} \right) \right]} \quad (\text{II-20})$$

To analyze the inhomogeneous plasma, a method described by Swift<sup>4</sup> is used. Using Swift's notation, the axial magnetic field with the plasma expressed as follows:

$$H_z^I(r, \phi) = \sum_{m=-\infty}^{\infty} \left[ \frac{G_{mz}(r)}{C_m} \right] C_m e^{-jm\phi} \quad (\text{II-21})$$

where the ratio  $\frac{G_{mz}(r)}{C_m} = t_m(r) + jU_m(r)$  is numerically evaluated to give solutions of  $t_m$  and  $u_m$  at the surface of the conducting cylinder,  $r = a$ . The details of the technique are adequately described in the reference and will not be repeated here.

At  $r = a$  the boundary condition at the aperture gives

$$\bar{E}_{m\phi}(a, \phi) = \frac{V_0}{2\pi a} \frac{\sin\left(\frac{m\phi_0}{2}\right)}{\left(\frac{m\phi_0}{2}\right)} = -\frac{C_m [t_m'(a) + ju_m'(a)]}{j\omega\epsilon(a)} \quad (\text{II-22})$$

which allows  $C_m$ , hence  $H_z^I(a, \phi)$  to be computed. Therefore, use of Parseval's theorem gives the following admittance expression

$$Y = -\frac{jk_0}{2\pi a} \frac{\epsilon(a)}{\epsilon_0} \sum_{m=-\infty}^{\infty} \frac{\sin^2\left(\frac{m\phi_0}{2}\right)}{\left(\frac{m\phi_0}{2}\right)^2} \left[ \frac{t_m(a) + ju_m(a)}{t_m'(a) + ju_m'(a)} \right] \quad (\text{II-23})$$

The prime in the above equation denotes differentiation with respect to  $r$ .

### APPENDIX III

#### RELATIONSHIP BETWEEN INTERNAL AND EXTERNAL ADMITTANCE

Computation of the external admittance is only half the story since the external admittance as such is not a measurable quantity; when an experiment is performed, the input admittance is referred through a measurement of the reflection coefficient. This input admittance (or reflection coefficient) as seen in the feed structure must be related to the external admittance. To do this, however, flow conservation immediately inside and outside the slot is used.

The pertinent fields which exist in the waveguide, due to the waveguide opening onto the ground plane, are

$$E_{\eta} = \vec{E}_0 e^{-j\beta_{01}z} \cos\left(\frac{\pi\xi}{l}\right) \left[1 + \Gamma e^{j2\beta_{01}z}\right] + (\text{h.t.})_E \quad (\text{III-1a})$$

$$H_{\xi} = -\vec{E}_0 Y_{01} e^{-j\beta_{01}z} \cos\left(\frac{\pi\xi}{l}\right) \left[1 - \Gamma e^{j2\beta_{01}z}\right] + (\text{h.t.})_H \quad (\text{III-1b})$$

Assuming that higher-order terms vanish, i.e.,  $(\text{h.t.})_E = (\text{h.t.})_H = 0$  the complex power flow expressed in terms of the fields inside the slot is

$$P_{c\eta} = |\vec{E}_0|^2 (1 + \Gamma^*)(1 - \Gamma) Y_{01} \frac{wl}{4} \quad (\text{III-2})$$

But,

$$\vec{E}_0 = \frac{V_0}{w} \frac{1}{1 + \Gamma} \quad (\text{III-3})$$

Therefore,

$$Y_c = \frac{2P}{|V_0|^2} = \frac{1}{w^2} \frac{(1 + \Gamma^*)(1 - \Gamma)}{|1 + \Gamma|^2} \frac{wl}{2} Y_{01} = \frac{l}{2w} \frac{(1 - \Gamma)}{(1 + \Gamma)} Y_{01} \quad (\text{III-4})$$

But, the input admittance is defined as

$$Y_{in} = -\frac{H_E}{E_\eta} = Y_{o1} \left( \frac{1 - \Gamma}{1 + \Gamma} \right) \quad (\text{III-5})$$

Therefore, the following relationship exists between the external and input admittance

$$Y_{in} = 2 \left( \frac{w}{l} \right) Y_c \quad (\text{III-6})$$

or, in normalized form,

$$y_{in} = \frac{Y_{in}}{Y_{o1}} = g_{in} + jb_{in} = 2 \left( \frac{w}{l} \right) \left( \frac{\lambda_{g01}}{\lambda_v} \right) y_{cv} \quad (\text{III-7})$$

Therefore equation III-7 relates a calculated normalized external admittance  $(y_{cv})$  to the measurable normalized input admittance  $y_{in}$ .

## REFERENCES

1. C. M. Knop and C. T. Swift, "A Note on the Radiation Conductance of an Axial Slot on a Cylinder," Radio Science, Journal of Research, NBS/USNC-URSI, vol. 69, No. 3, pp. 447-451, March 1965.
2. J. R. Wait, Electromagnetic Radiation From Cylindrical Structures, Pergamon Press, New York, New York, 1959.
3. R. F. Harrington, Time Harmonic Electromagnetic Fields, McGraw-Hill Book Company, New York, New York, 1961.
4. C. T. Swift, and C. M. Knop, "Equatorial Patterns of an Axially Slotted Cylinder Coated with a Critical Dense Plasma," IEEE, PTGAP, vol. AP-12 (Communications), pp. 498-502, July 1964.
5. C. T. Swift, "Radiation Patterns of a Slotted-Cylinder Antenna in the Presence of an Inhomogeneous Lossy Plasma," IEEE, PTGAP, vol. AP-12, no. 6, pp. 728-738, Nov. 1964.
6. J. R. Wait, "Radiation Characteristics of Axial Slots on a Conducting Cylinder," Wireless Engineer, vol. 32, no. 12, December 1955.
7. Y. Musiaka and R. E. Webster, "Radiation Characteristics with Power Gain for Slots on a Sphere," IRE Transactions on Antenna and Propagation, vol. AP-5, no. 1, January 1957.
8. C. T. Swift, "Radiation from Slotted-Cylinder Antennas Coated with Concentric Layers of Dielectric Material," M. Sc. Thesis, Virginia Polytechnic Institute, April 1965.

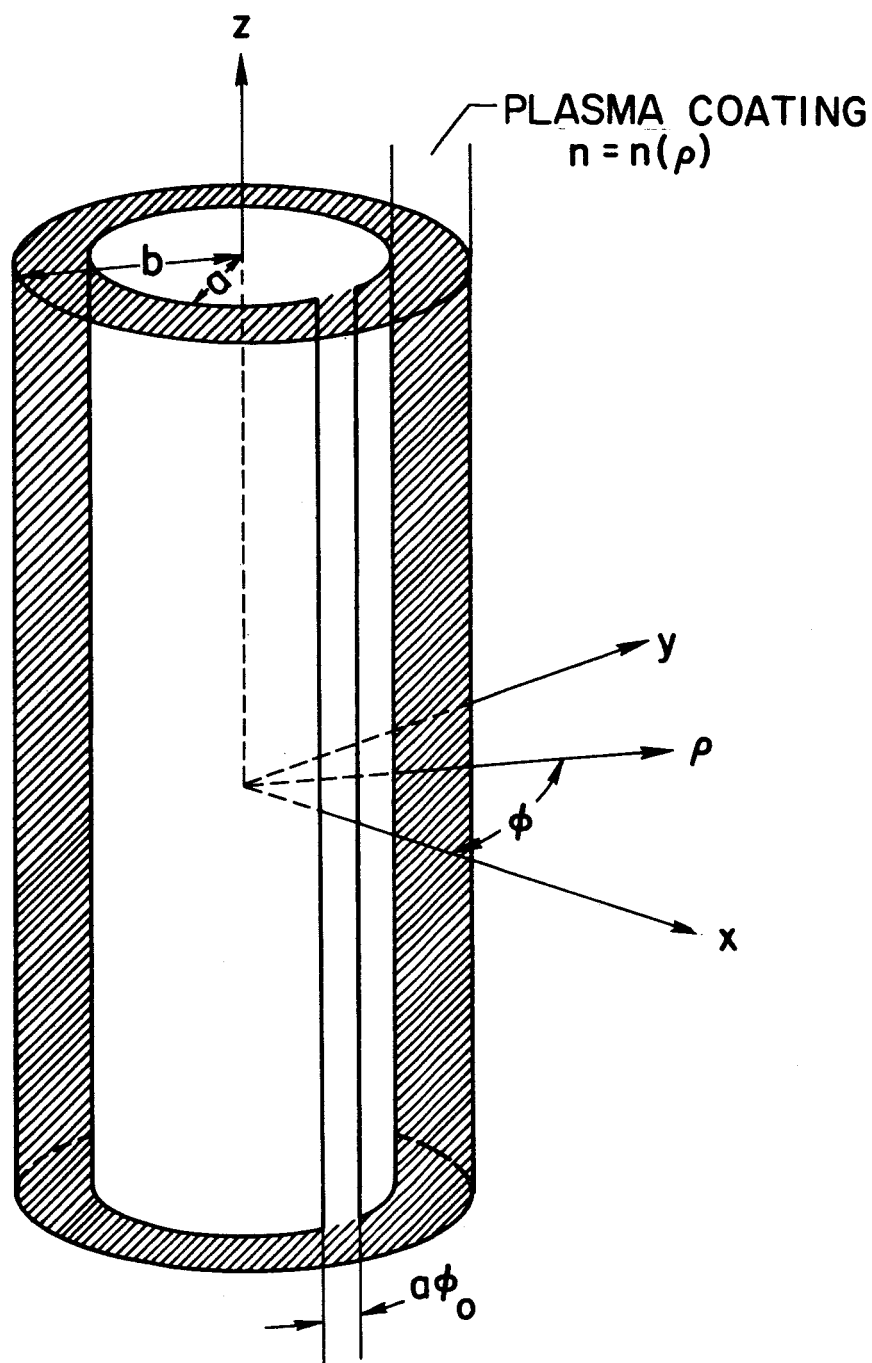


TABLE I.- MEASUREMENTS OF INPUT ADMITTANCE FOR DIFFERENT DIELECTRIC SLEEVE POSITIONS

Sleeve position	Frequency, kmc	VSWR	D <sub>c</sub> , cm	D <sub>sl</sub> , cm	$\Delta = D_{sl} - D_c$ , cm	$\frac{\Delta}{\lambda_g}$	g <sub>in</sub>	b <sub>in</sub>
		With coating	With short					
A	10.60	1.92	14.41	14.51	0.10	0.028	1.78	0.44
B	10.60	1.77	14.43	14.51	.09	.025	1.58	.50
C	10.60	1.77	14.46	14.51	.05	.014	1.75	.20
D	10.60	1.38	14.50	14.51	.01	.003	1.60	.03
A	10.80	2.35	14.78	14.89	0.11	0.031	2.02	0.76
B	10.80	2.00	14.79	14.89	.10	.028	1.84	.50
C	10.80	1.68	14.86	14.89	.03	.009	1.68	.12
D	10.80	1.37	14.96	14.89	-.07	-.020	1.37	-.11
A	11.00	2.4	15.21	15.23	0.02	0.006	2.4	0.20
B	11.00	2.1	15.12	15.23	.11	.032	1.86	.61
C	11.00	1.60	15.16	15.23	.07	.020	1.57	.20
D	11.00	1.72	15.27	15.23	-.04	-.012	1.72	-.16
A	11.20	1.85	13.91	13.90	-0.01	+0.003	1.88	-0.03
B	11.20	1.86	13.86	13.90	+.64	+.012	1.85	+.20
C	11.20	1.65	13.91	13.90	-.01	-.003	1.67	-.03
D	11.20	1.40	13.98	13.90	-.08	-.024	1.37	-.13
Position of Dielectric Sleeve			A	B	C	D		
Seam Location, Degrees from Slot			180	270	0	90		

TABLE II.- TABLES OF MODAL IMPEDANCE OF GAP ANTENNA

m	$g_m^e$	$b_m^e + b_m^i$	$Z_m$ , ohms
0	8.23	27.1	3.9 - j12.7
1	7.06	-.66	53 + j5.1
2	4.02	48.8	.6 + j7.7
3	1.11	-107	j3.5
4	.149	-168	j2.3
5	.011	-229	j2.0
6		-292	j1.6
7		-355	j1.4
8		-420	j.9
9		-486	j.8



NASA

Figure 1.- Geometry of coated slotted cylinder.

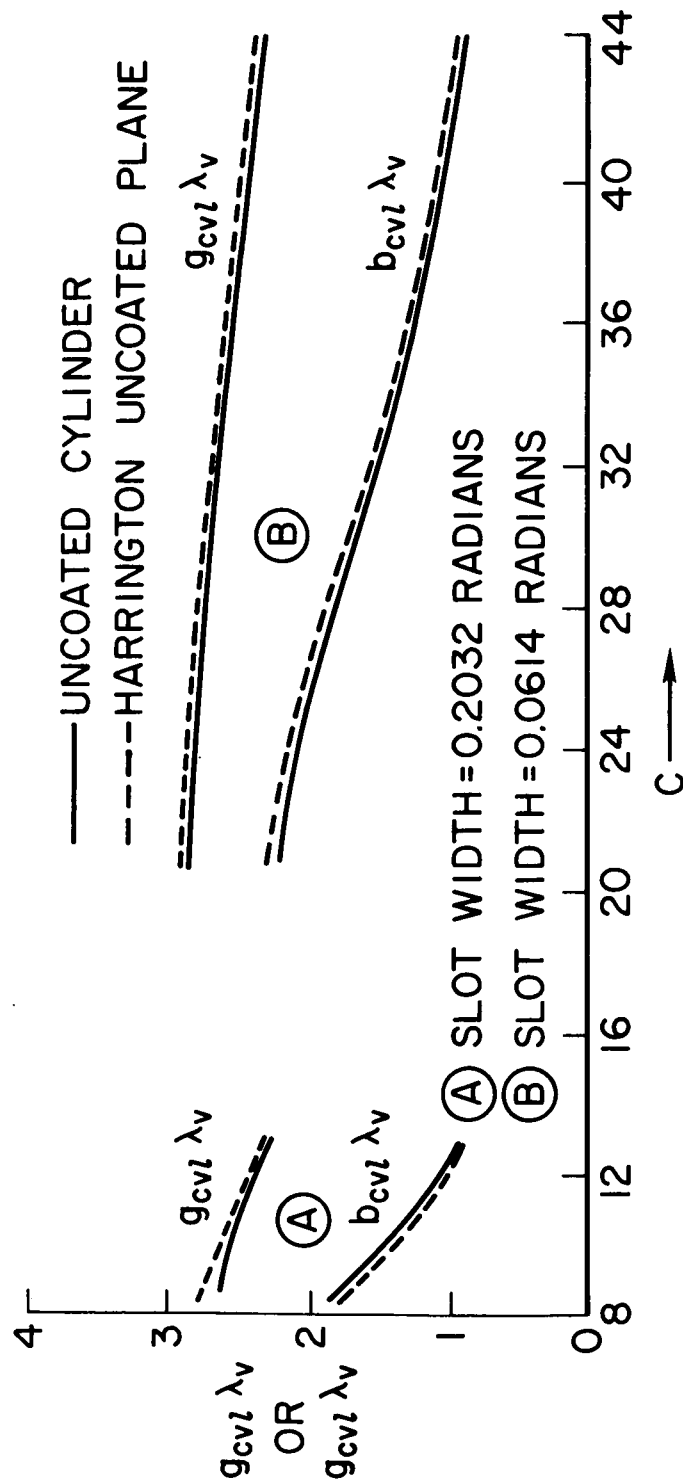
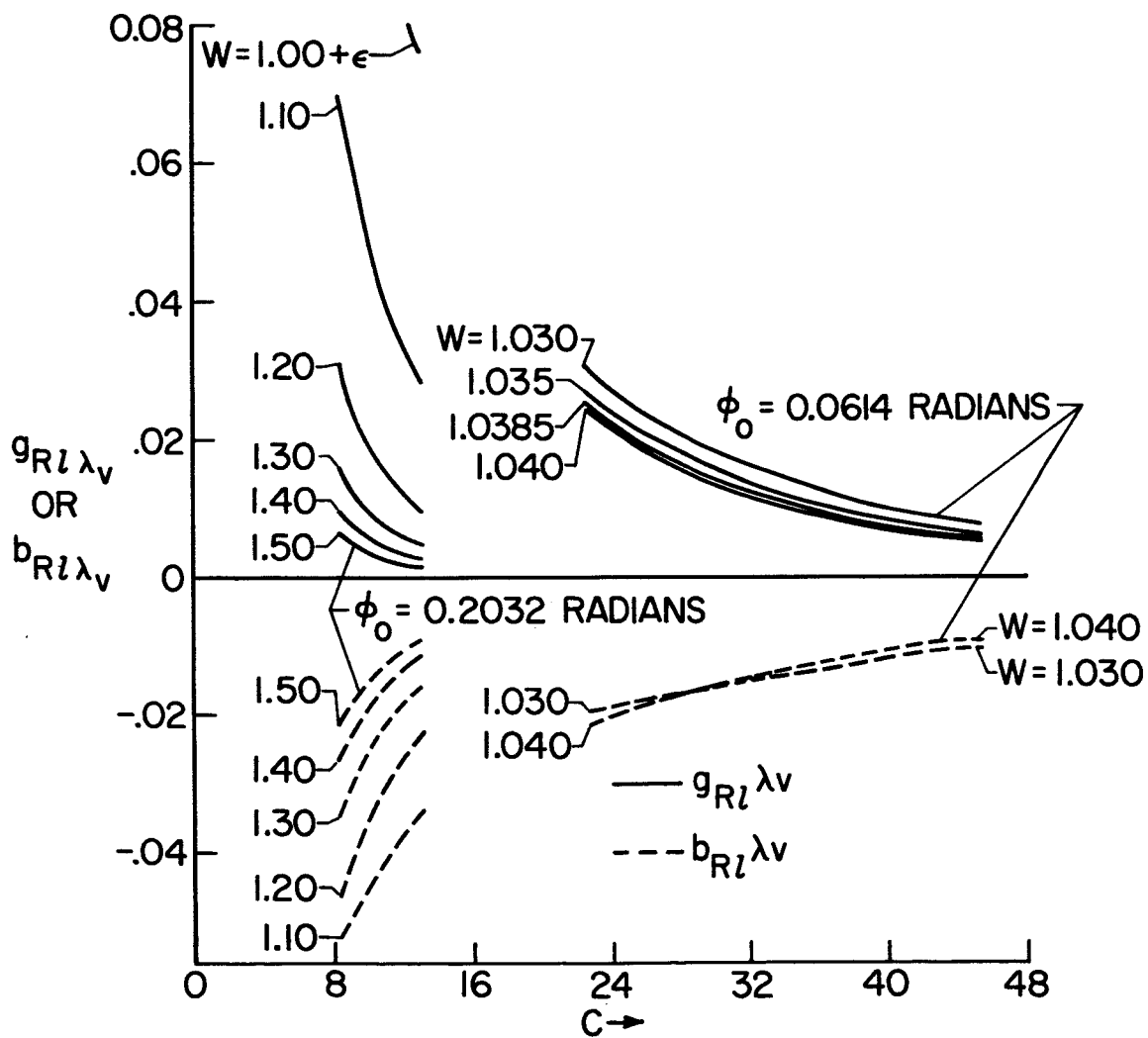
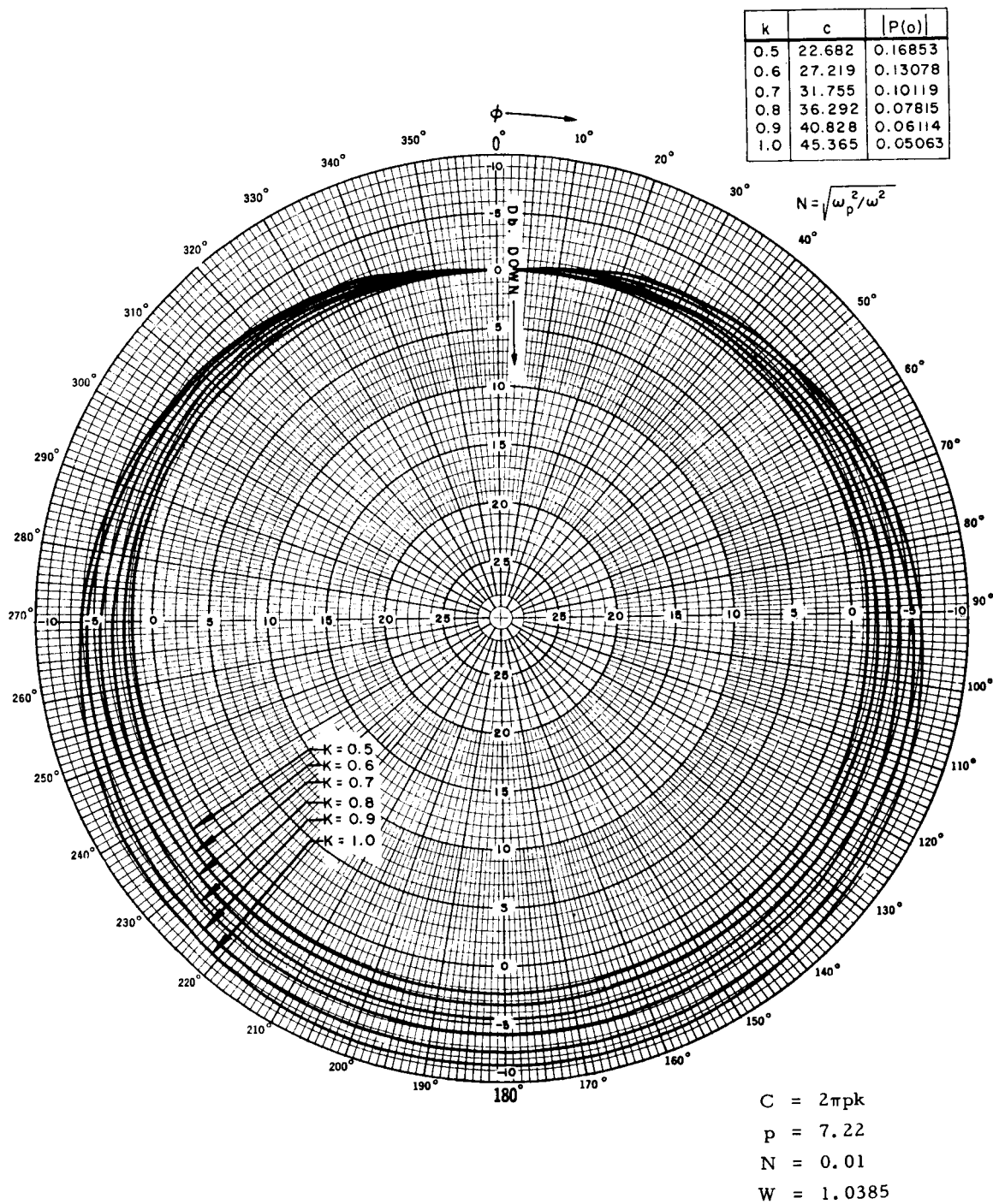


Figure 2.- Admittance of uncoated cylinder.



NASA

Figure 3.- Admittance at plasma resonance.



NASA

Figure 4.- Equatorial radiation patterns near plasma resonance.

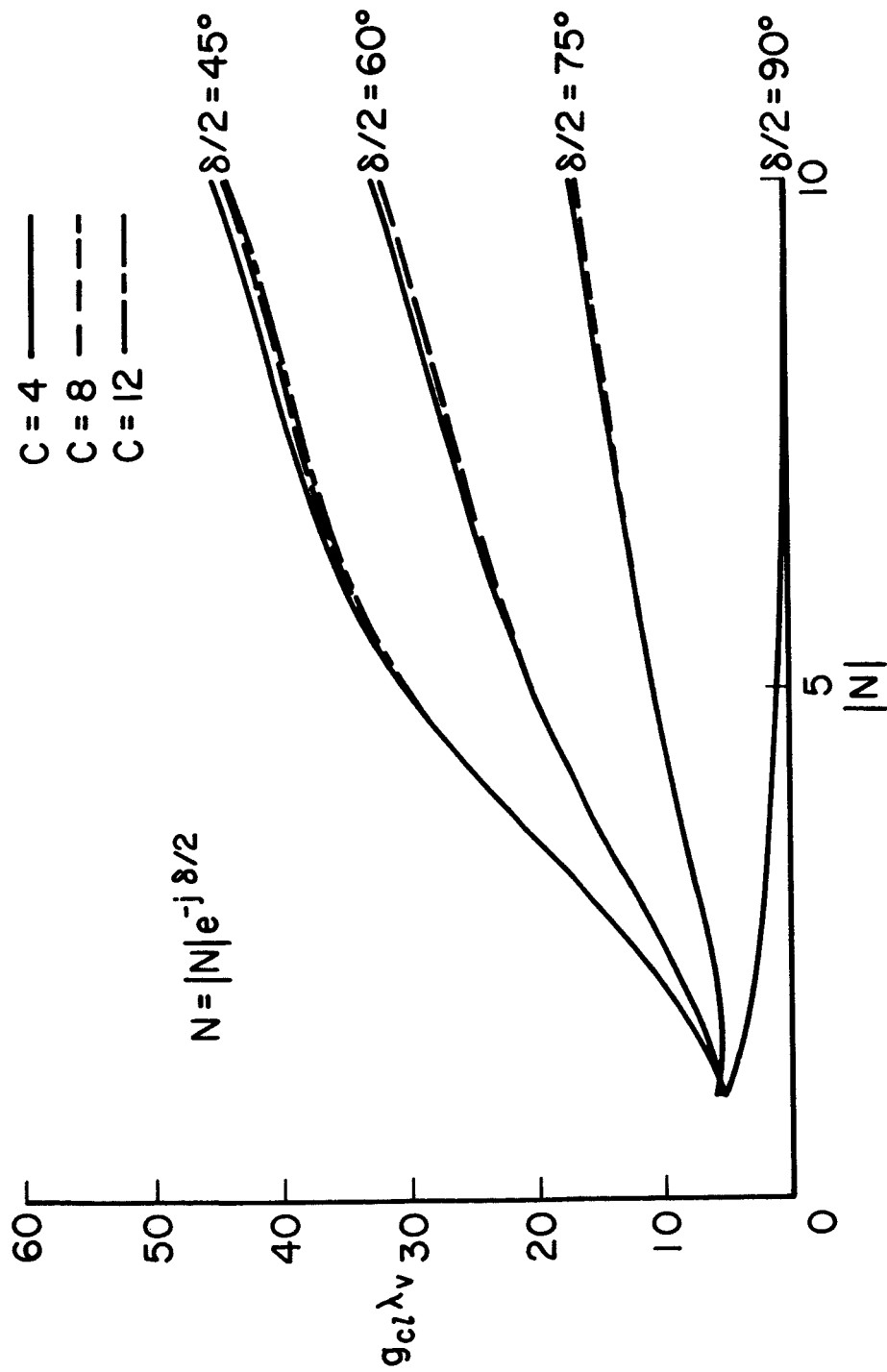
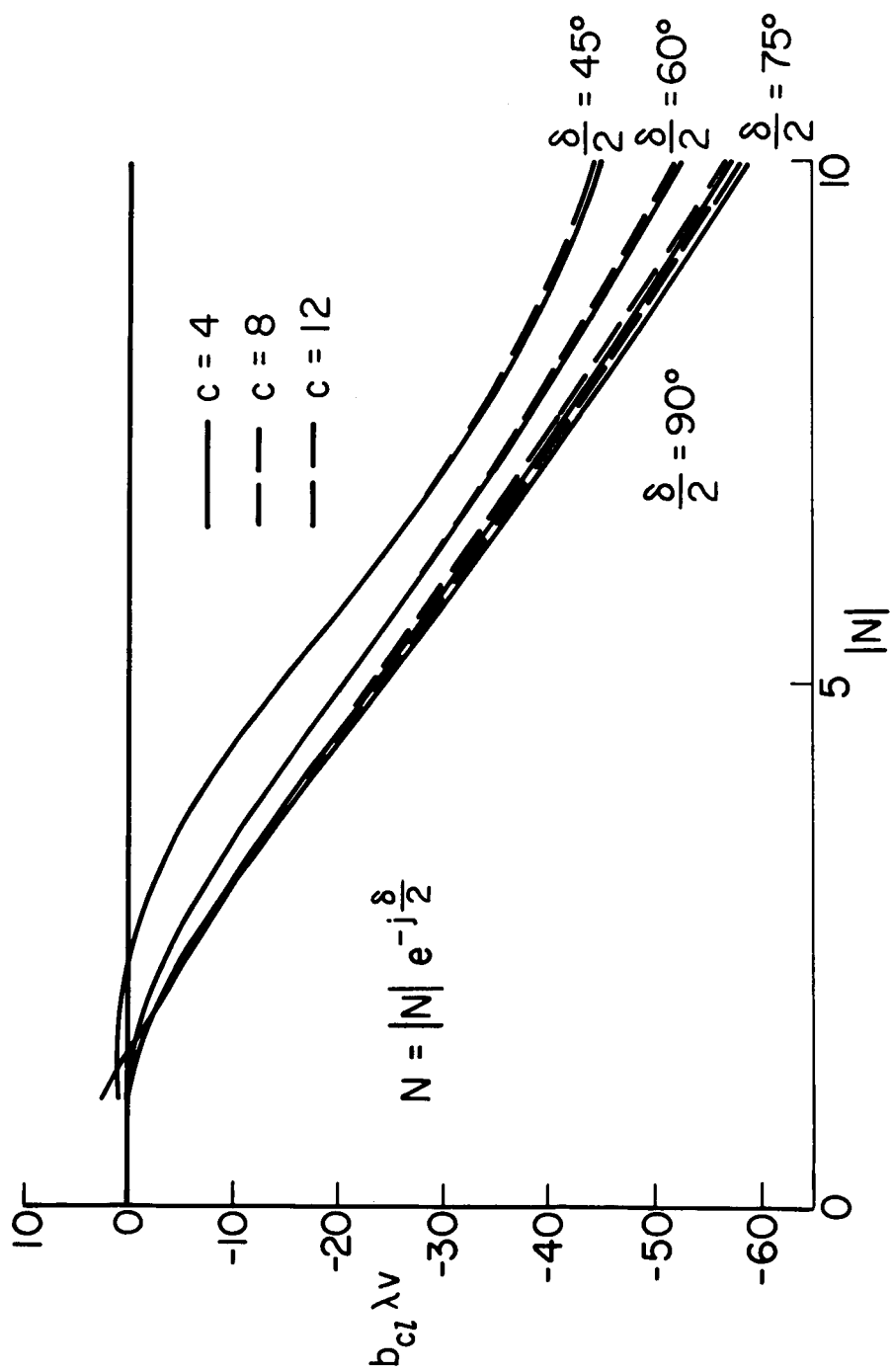


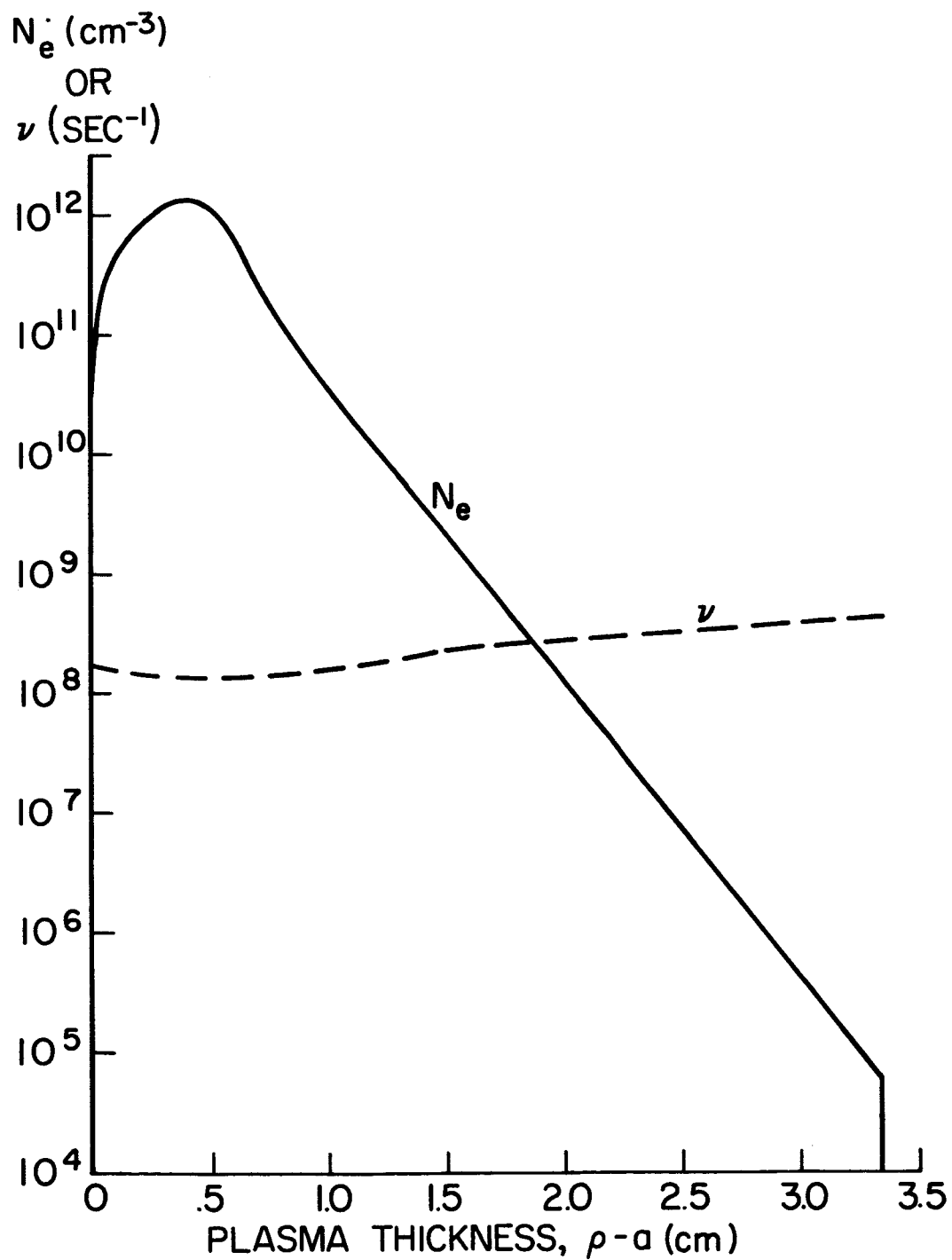
Figure 5.- Conductance with lossy coating.



NASA

Figure 6.- Susceptance with lossy coating.





NASA

Figure 7.- Typical reentry plasma profile.

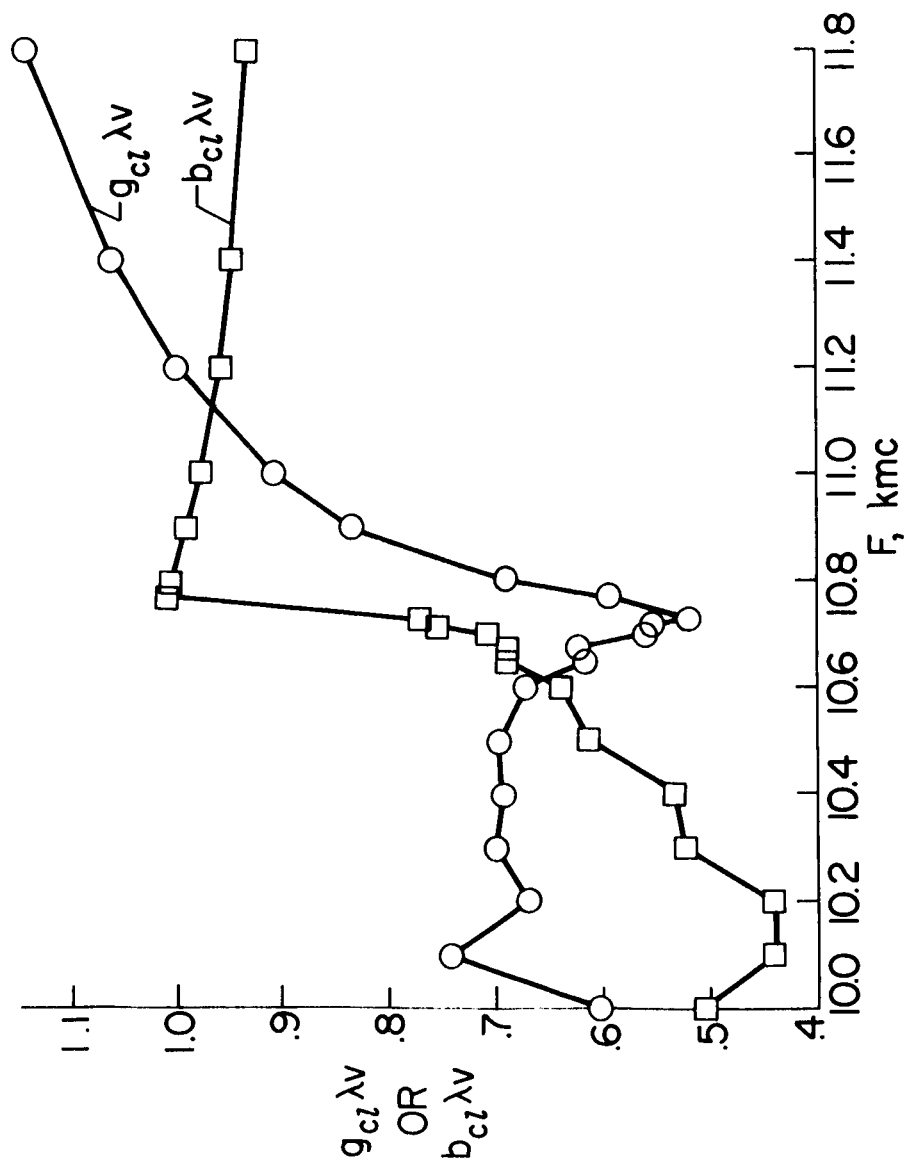
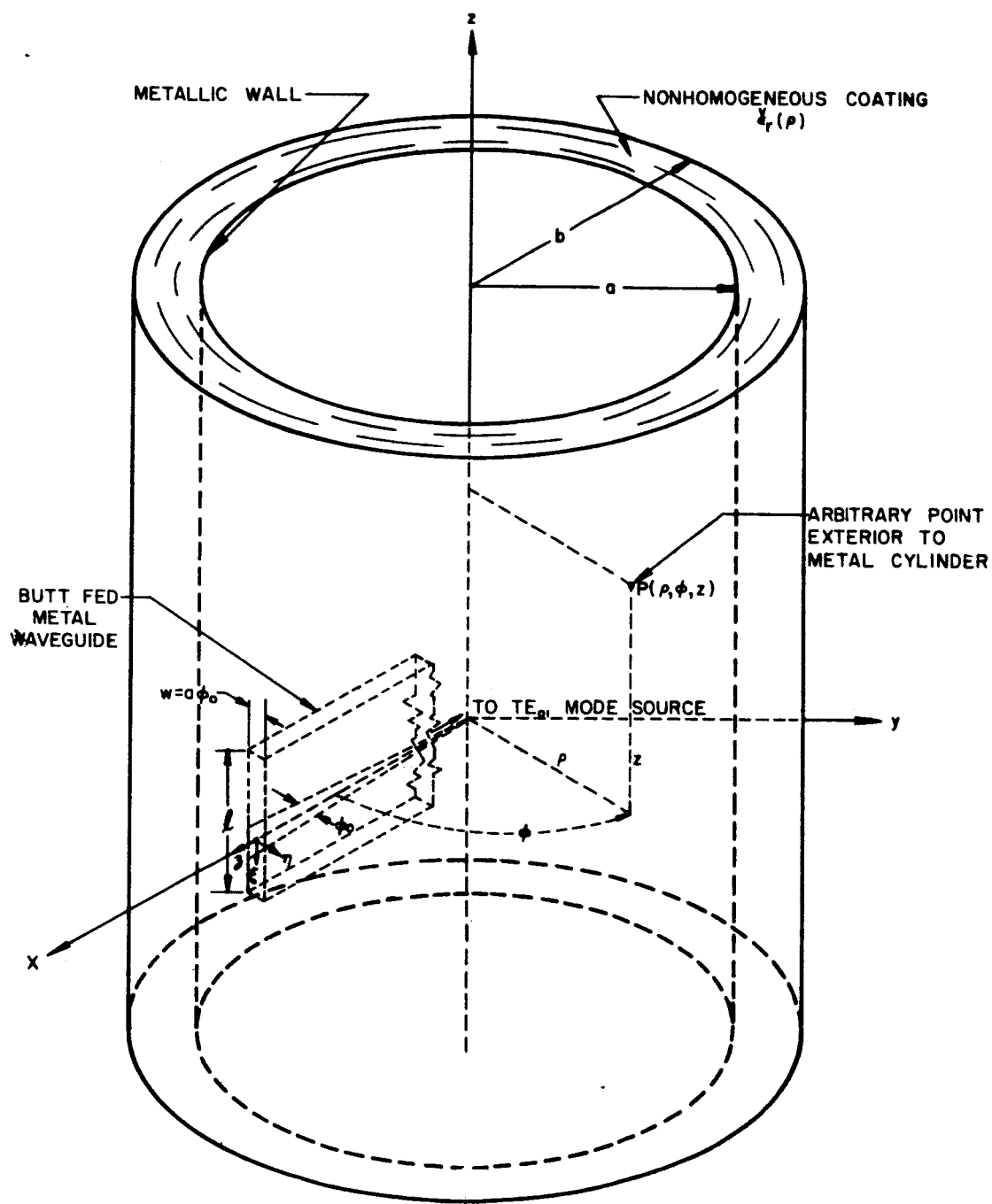
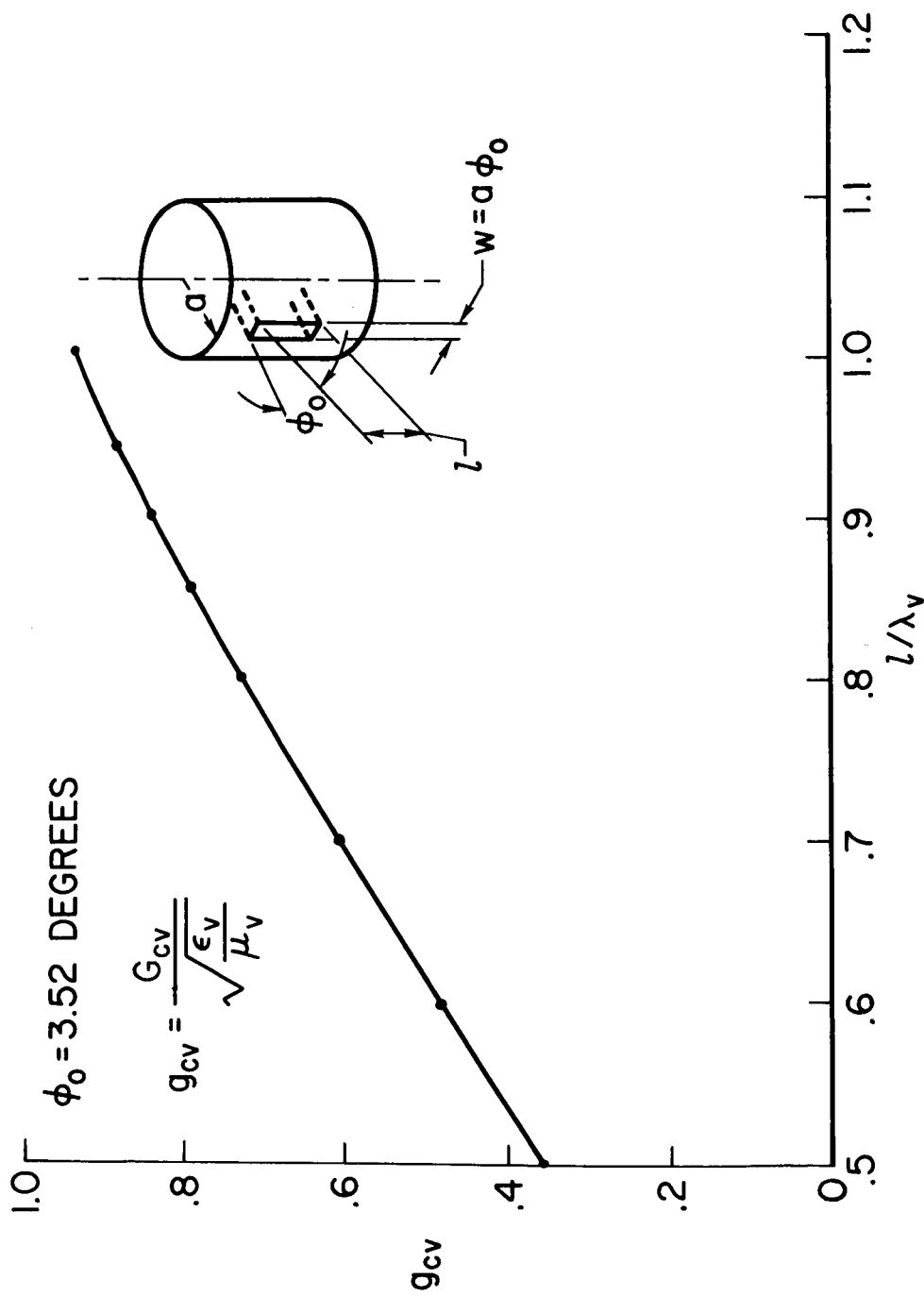


Figure 8.- Admittance of coated slots.



NASA

Figure 9.- Waveguide excited axial slot.



NASA

Figure 10.- External conductance of uncoated axial slot.

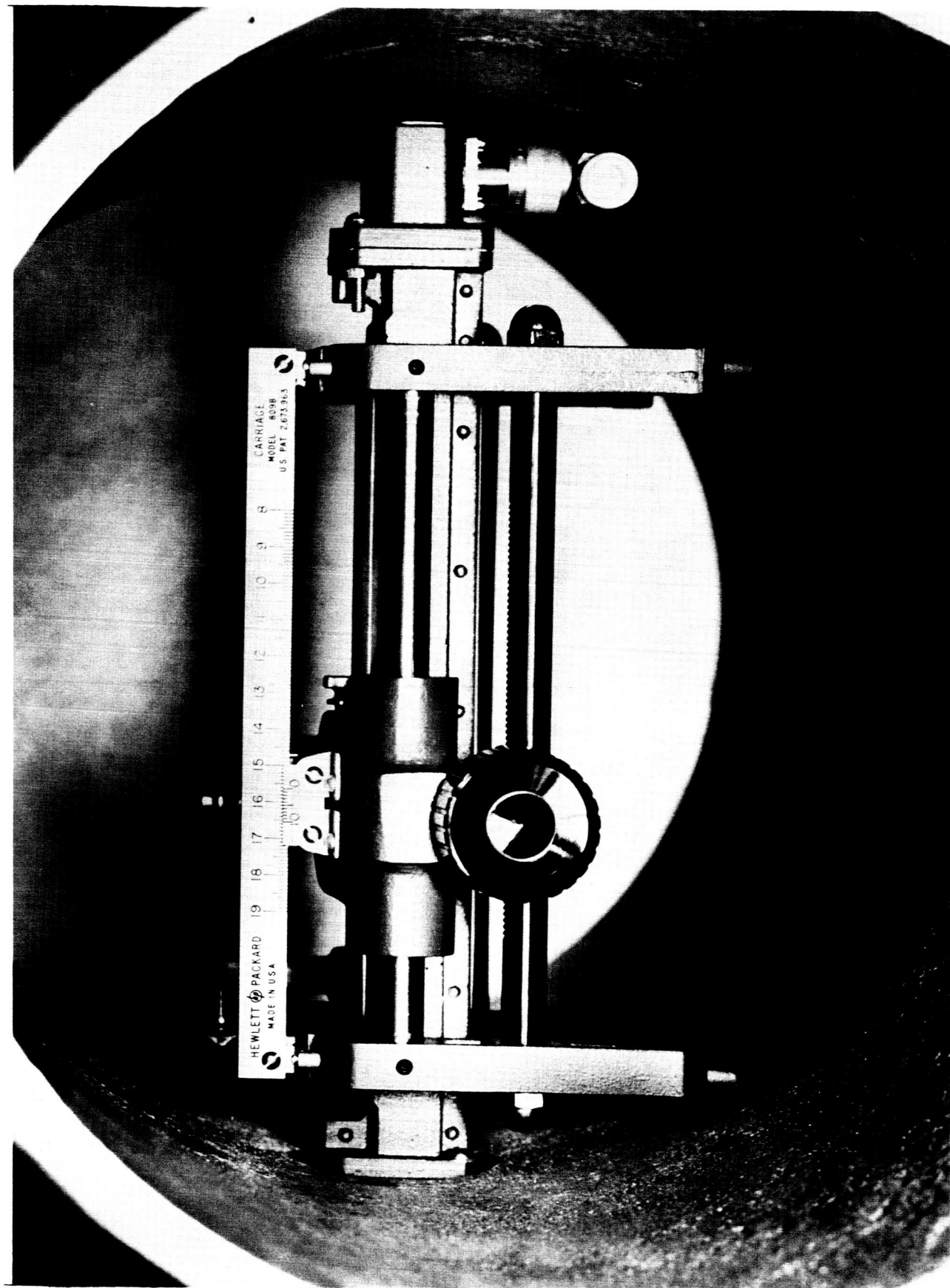
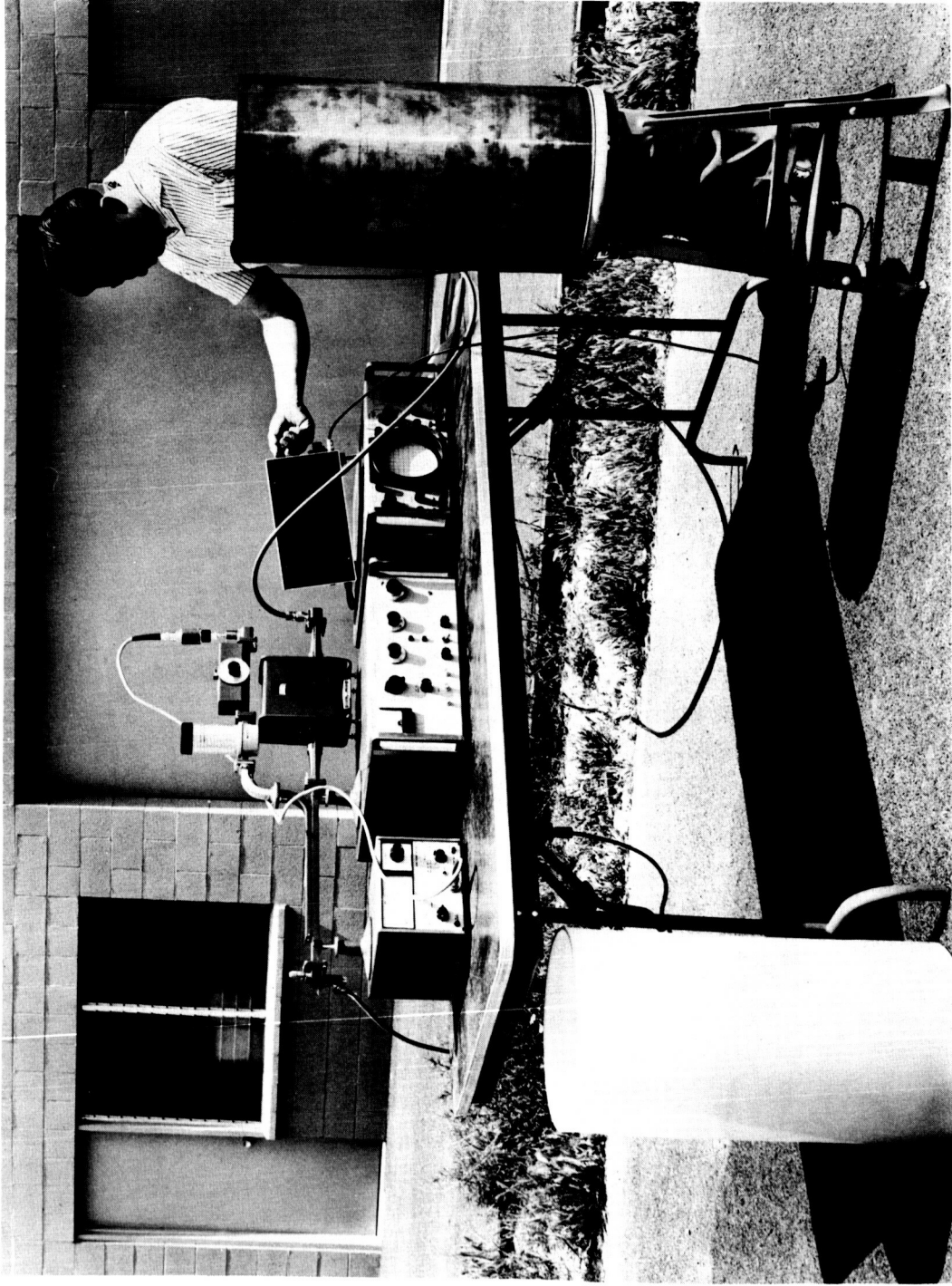


Figure 11.- Slotted line mounted inside cylinder.



NASA

Figure 12.- Experimental setup.

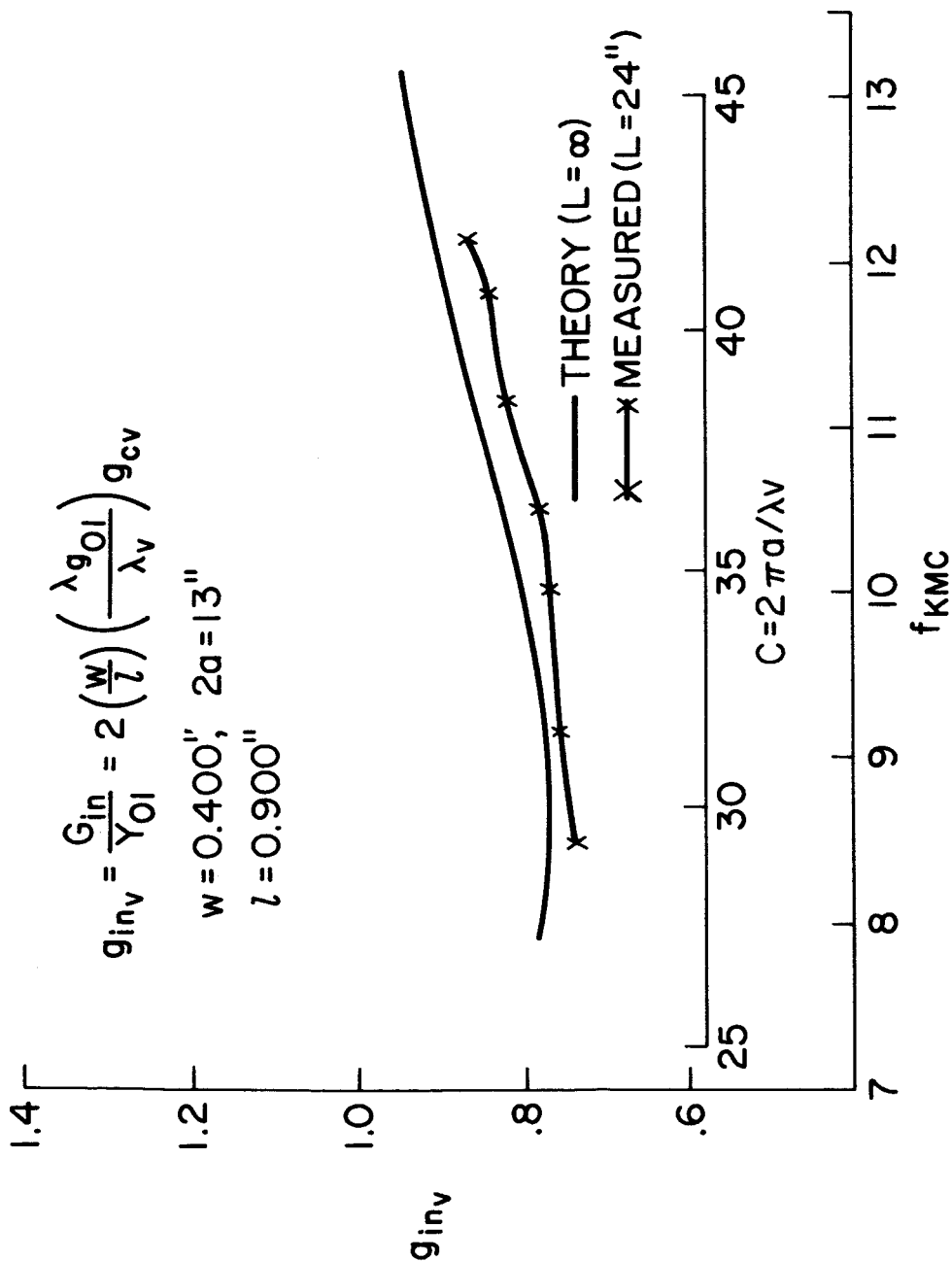
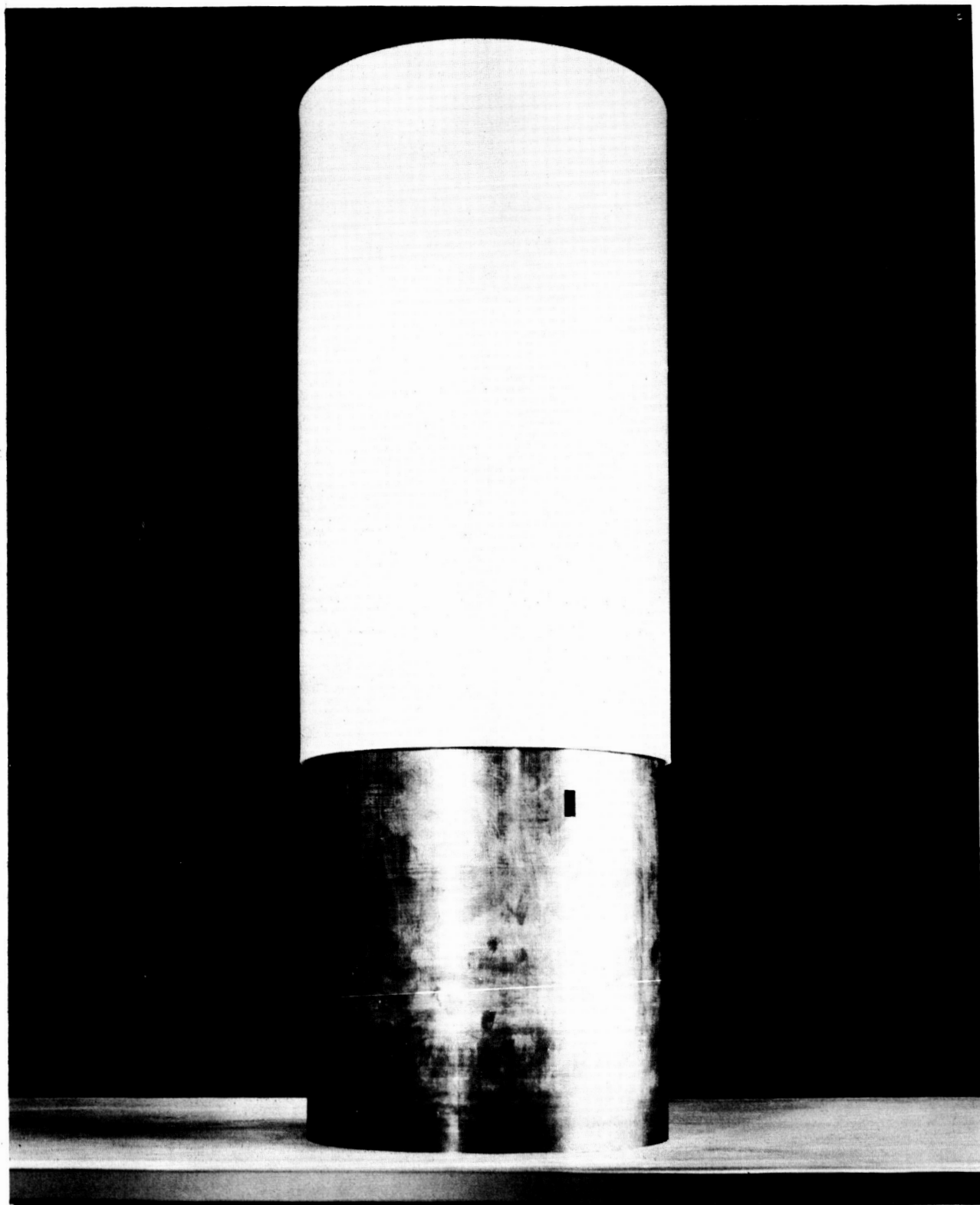


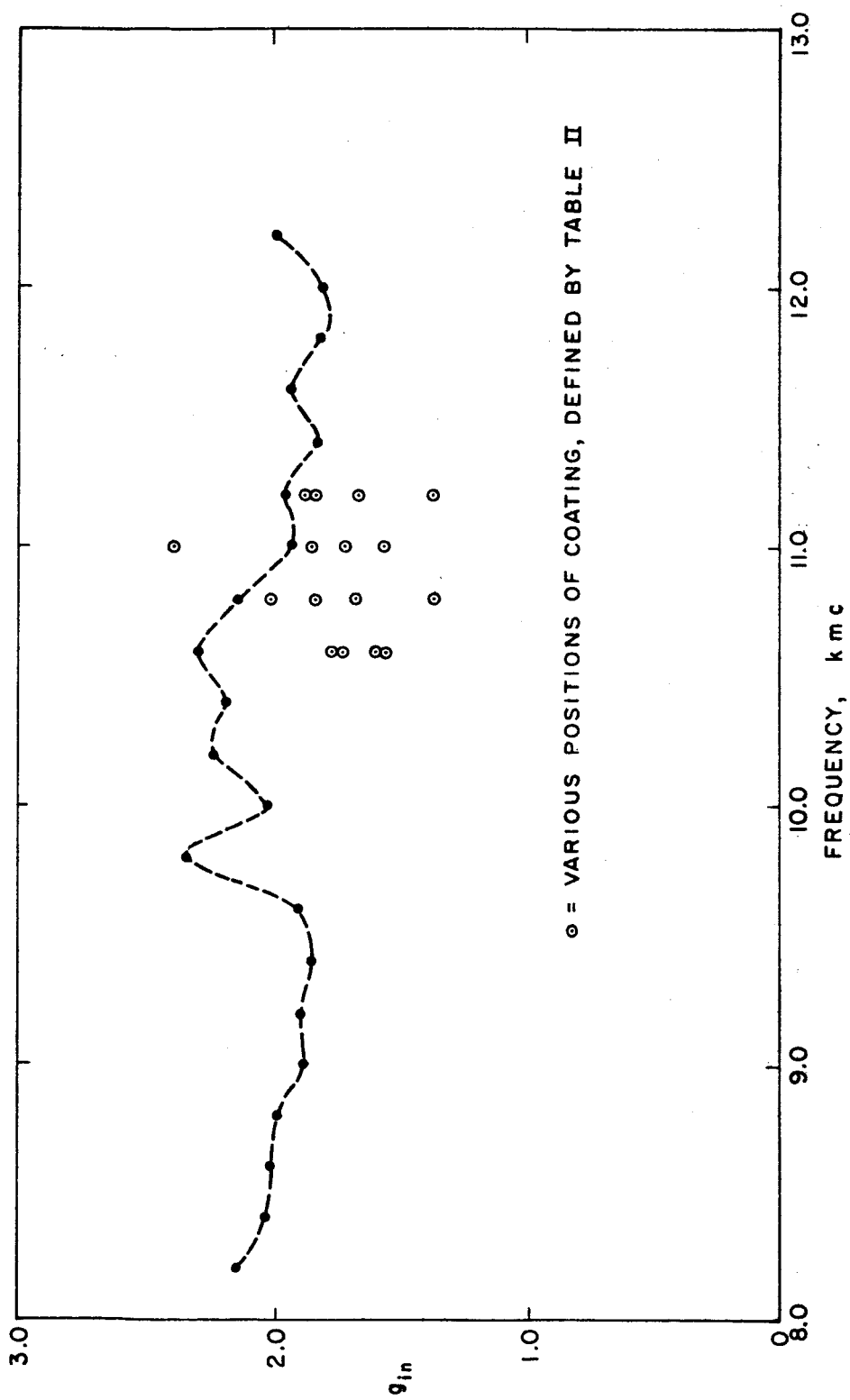
Figure 13.- Waveguide conductance of uncoated axial slot.



NASA

Figure 14.- Dielectric sleeve on metal cylinder.





NASA

Figure 15.- Waveguide conductance of coated axial slot.

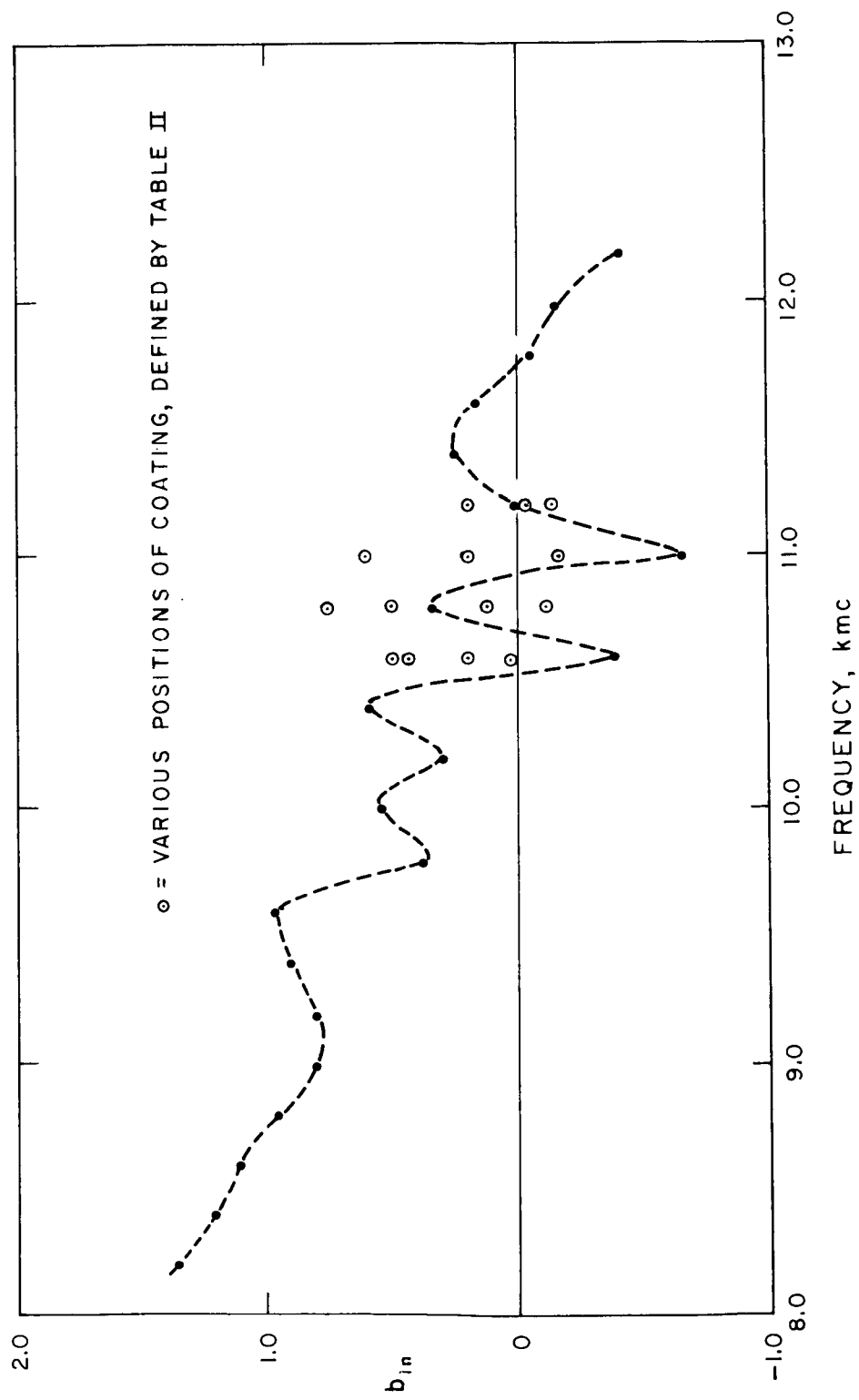
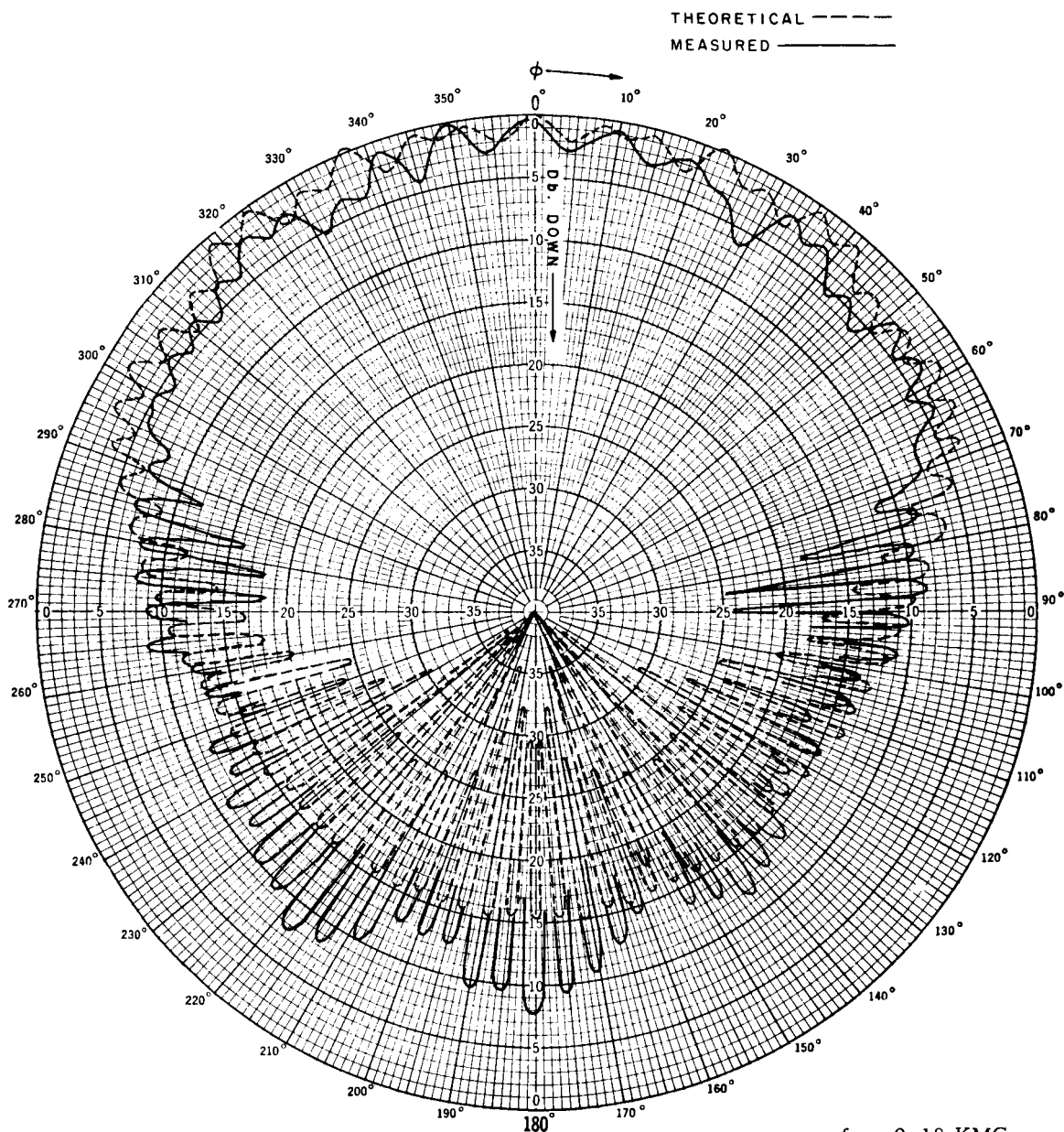


Figure 16.- Waveguide susceptance of coated axial slot.





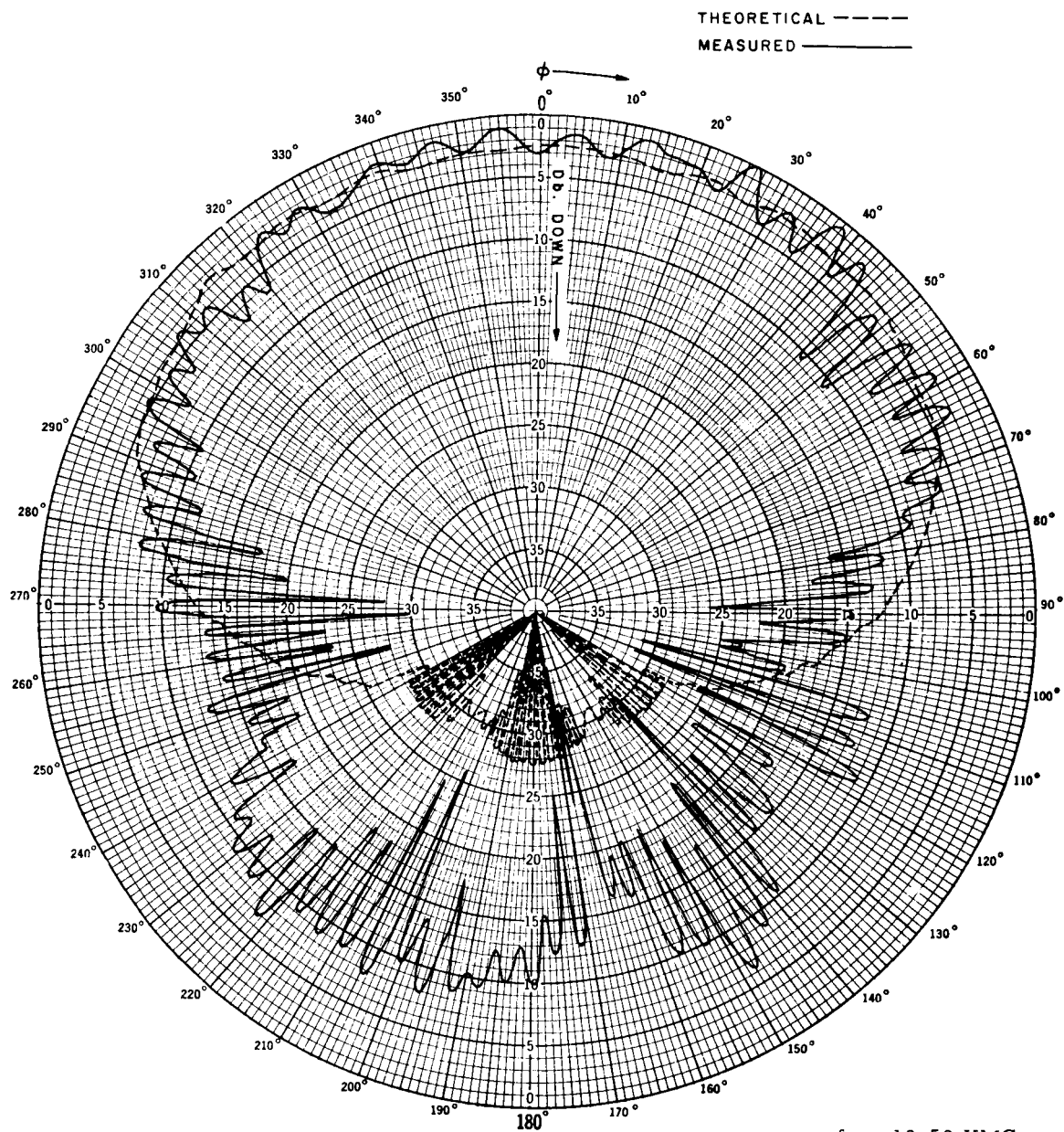
$f = 9.18 \text{ KMC}$   
 $W = 1.0385$   
 $N = 1.50$   
 $k = 0.7$   
 $|P(o)| = 5.1263$

(b)  $k = 0.7$ .

NASA

Figure 17.- Continued.



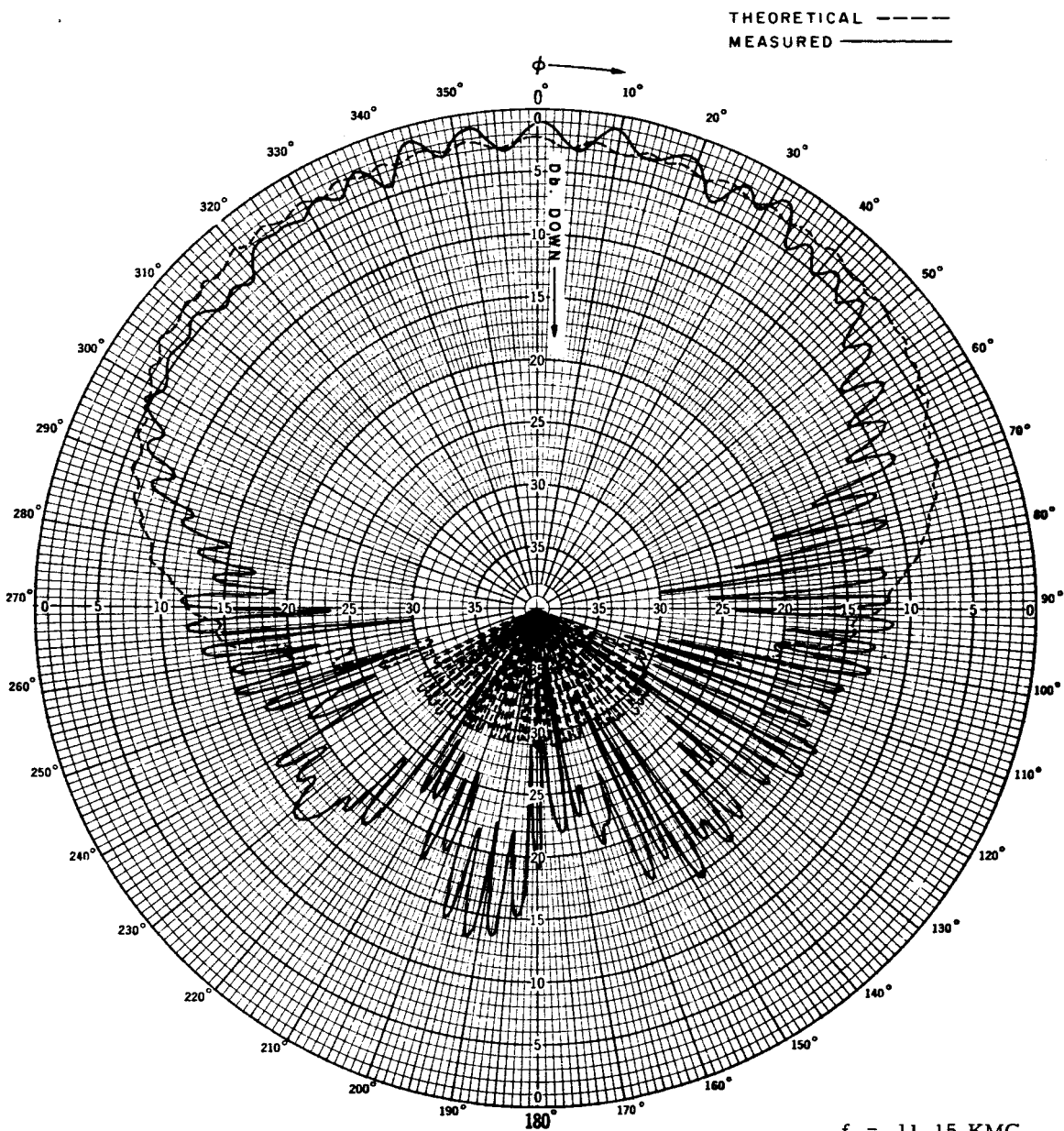


$f = 10.50 \text{ KMC}$   
 $W = 1.0385$   
 $N = 1.50$   
 $k = 0.80$   
 $|P(0)| = 4.194$

(d)  $k = 0.80$ .

NASA

Figure 17.- Continued.

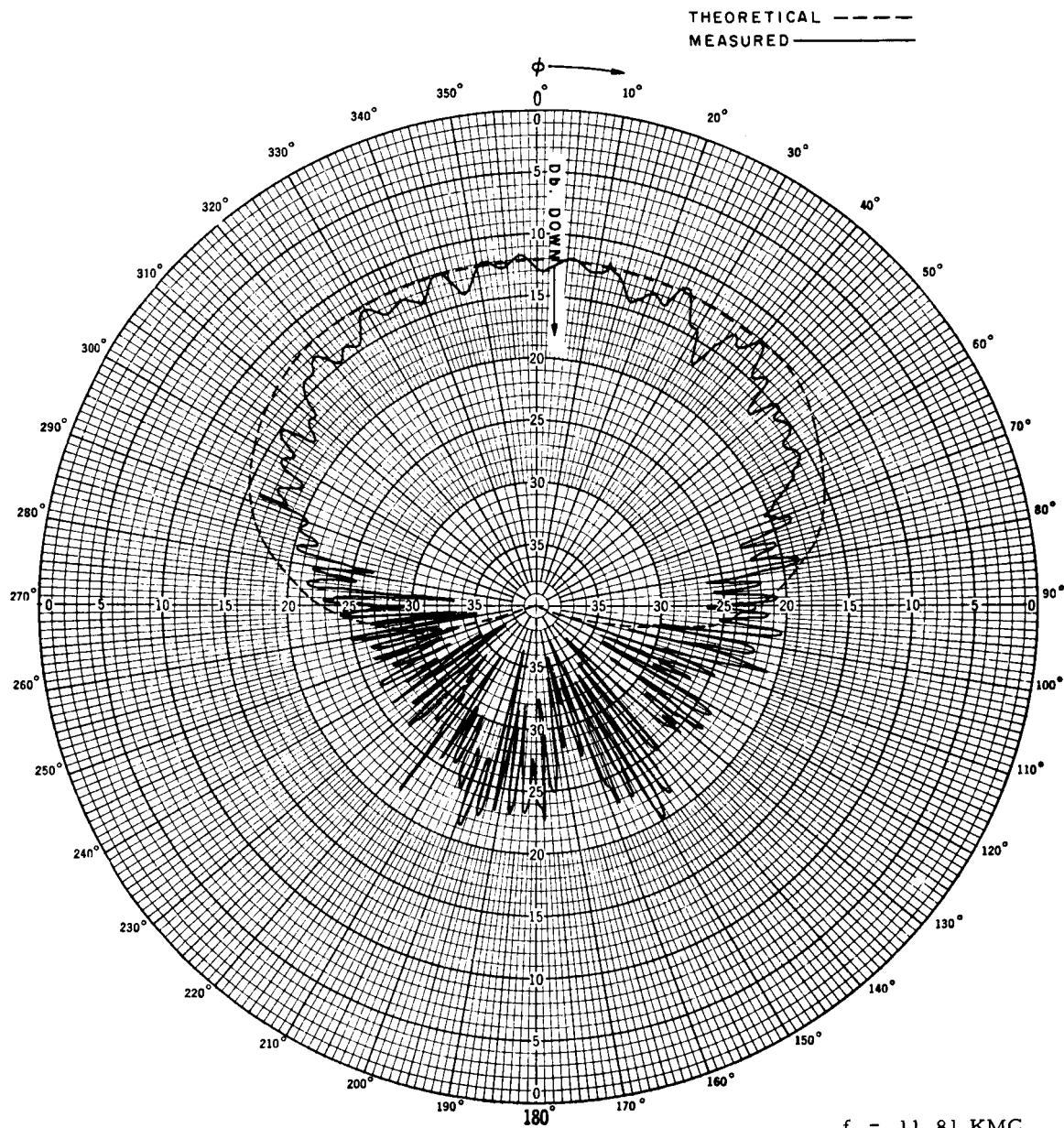


$f = 11.15 \text{ KMC}$   
 $W = 1.0385$   
 $N = 1.50$   
 $k = 0.85$   
 $P(o) = 4.06289$

(e)  $k = 0.85$ .

NASA

Figure 17.- Continued.



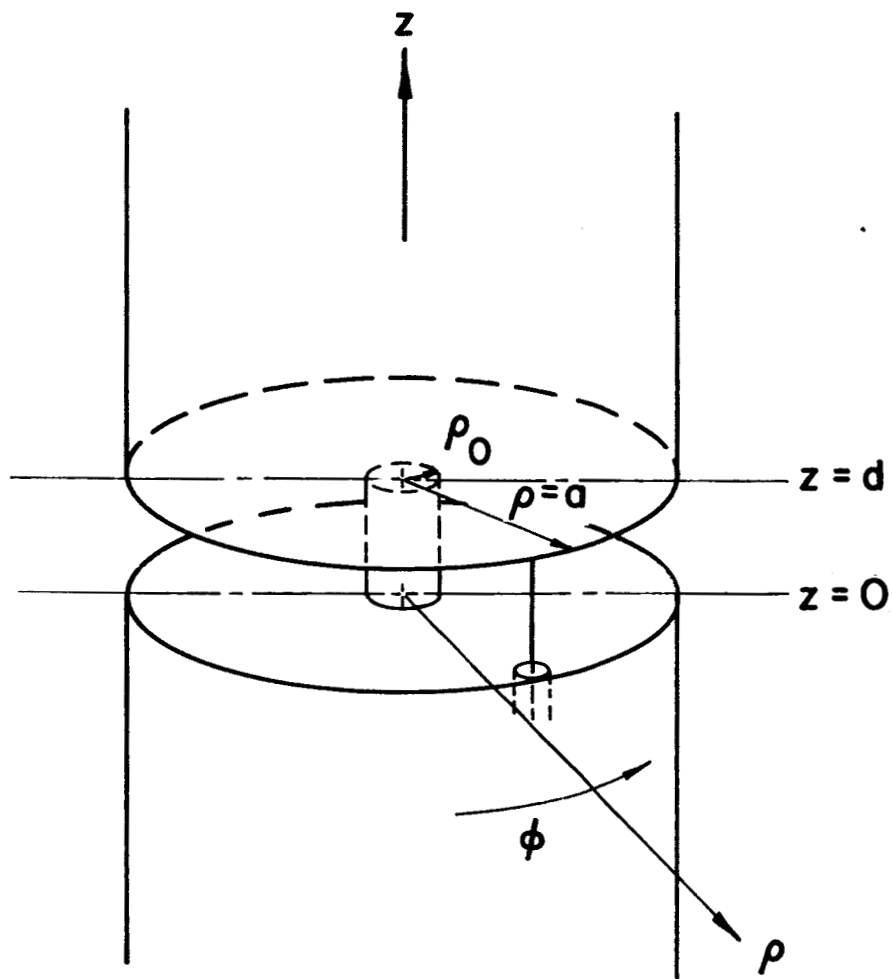
$f = 11.81 \text{ KMC}$   
 $W = 1.0385$   
 $N = 1.50$   
 $k = 0.90$   
 $|P(o)| = 3.7323$

(f)  $k = 0.90$ .

NASA

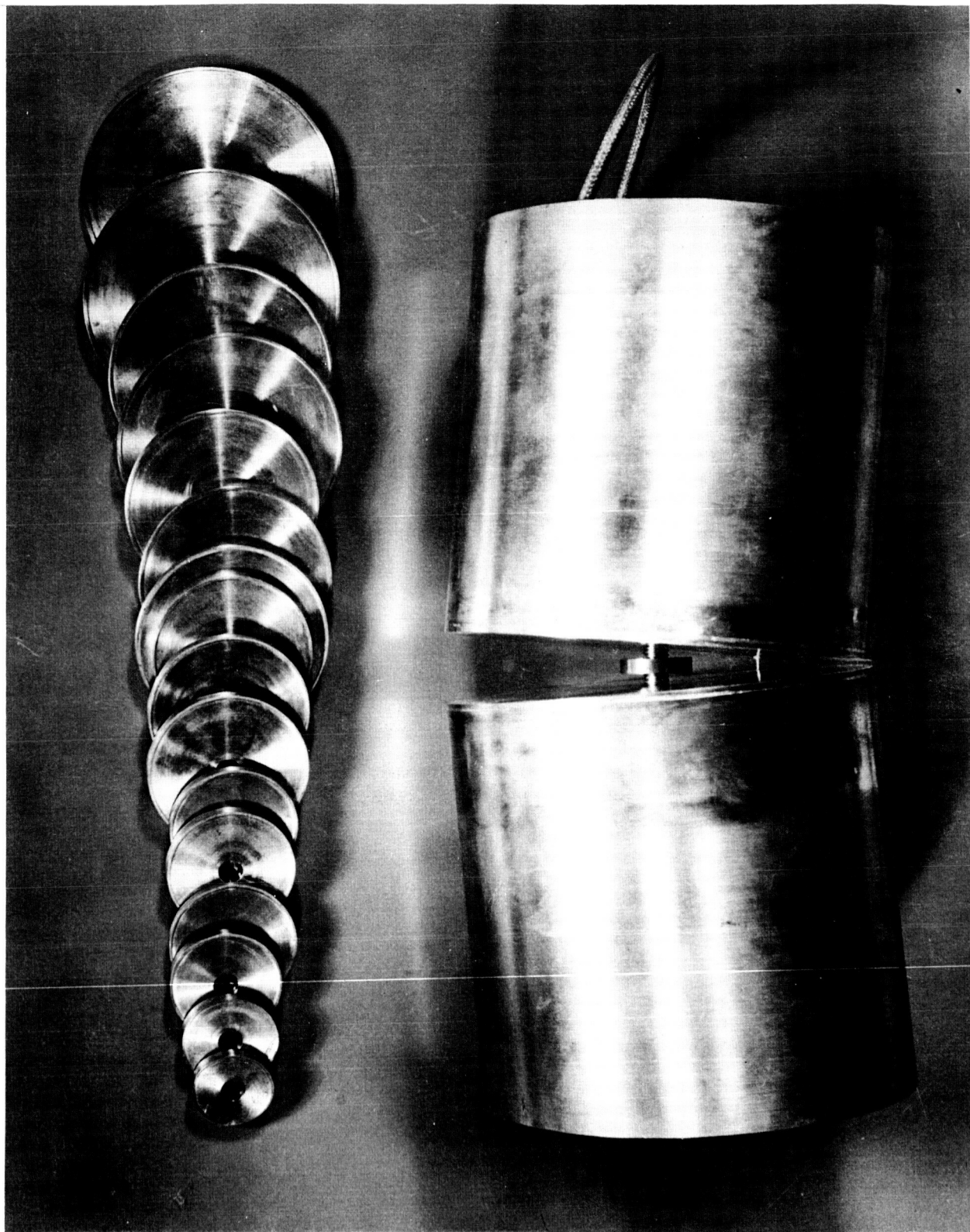
Figure 17.- Concluded.





NASA

Figure 18.- Cylindrical gap antenna.



NASA

Figure 19.- Exploded view of the gap antenna with spacers.

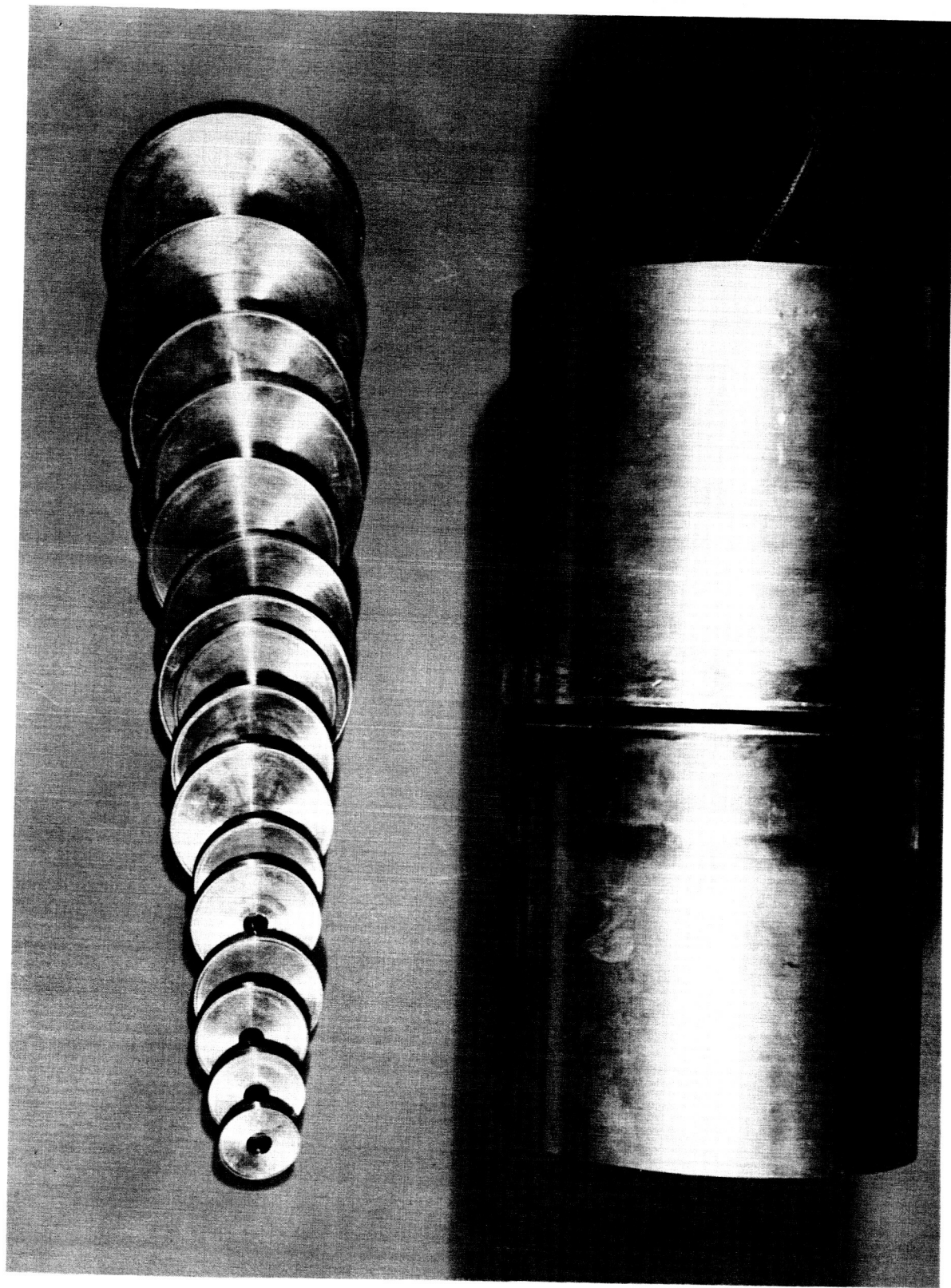
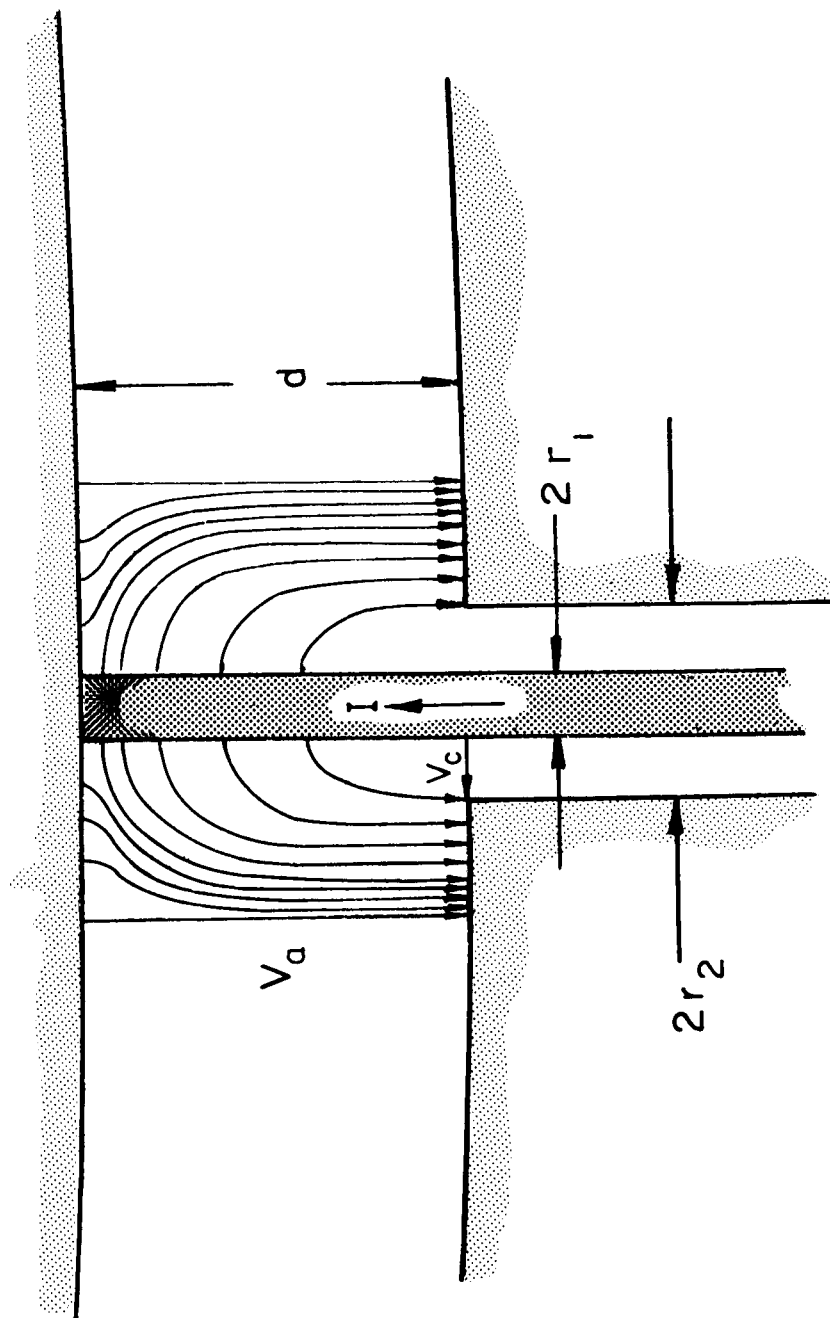
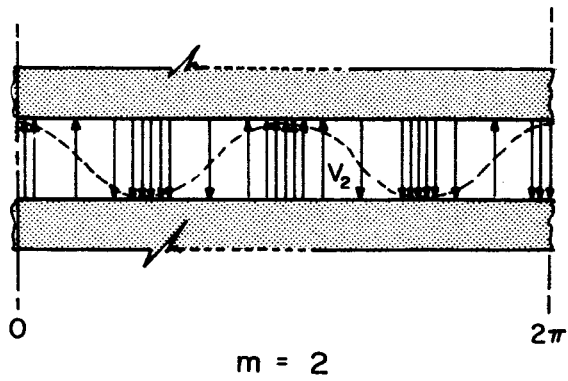
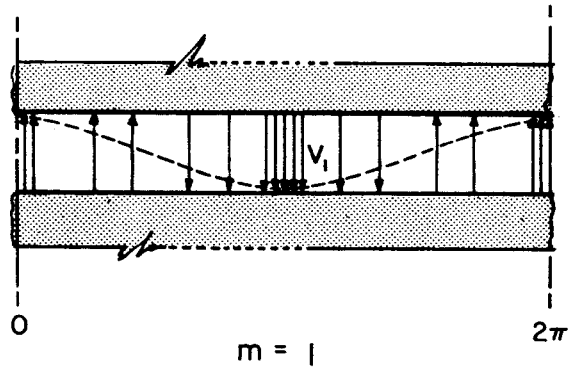
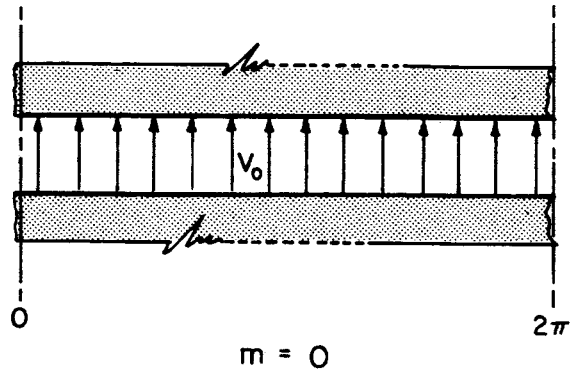


Figure 20.- Assembled gap antenna with spacers.



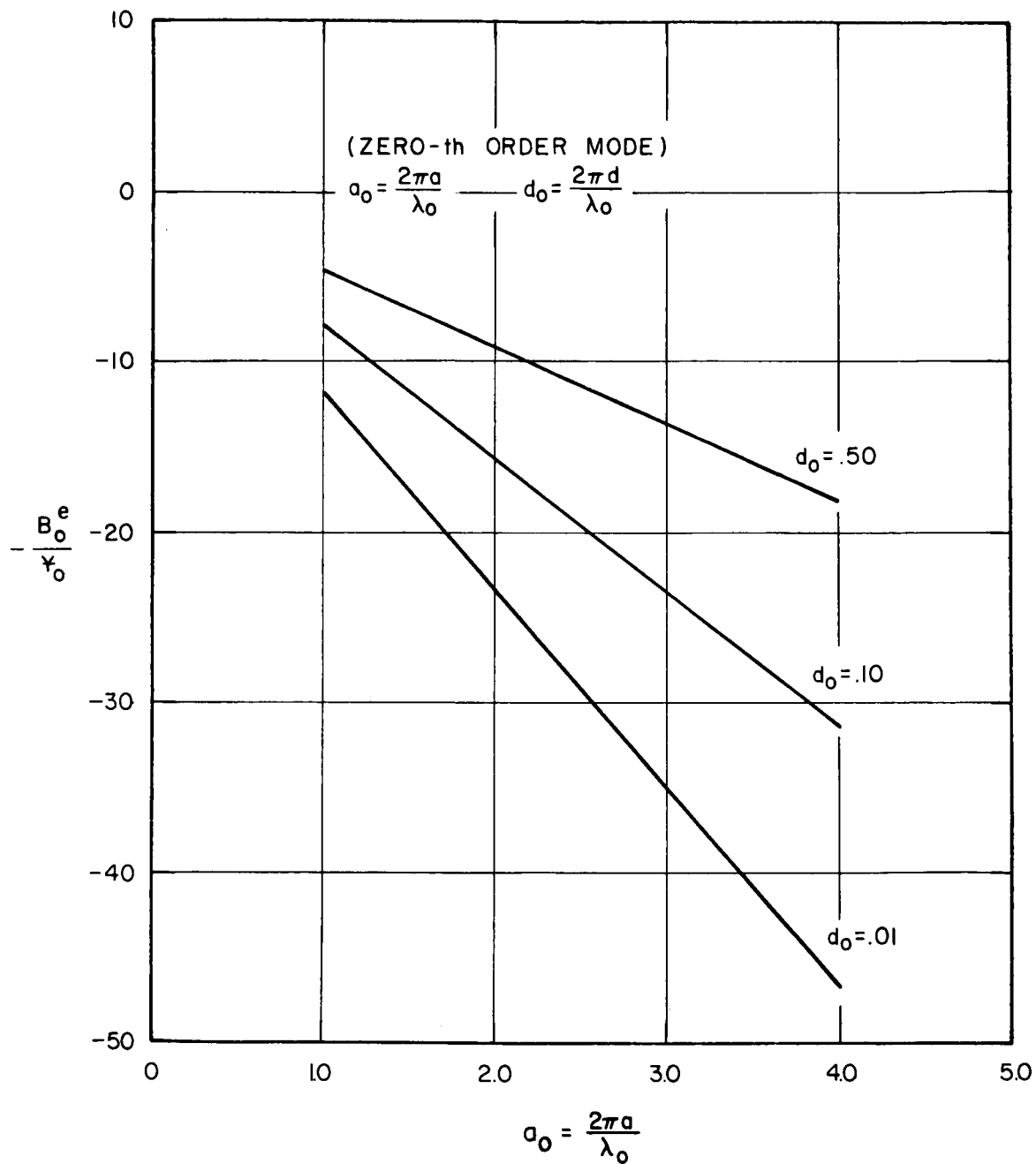
NASA

Figure 21.- Gap antenna feed.



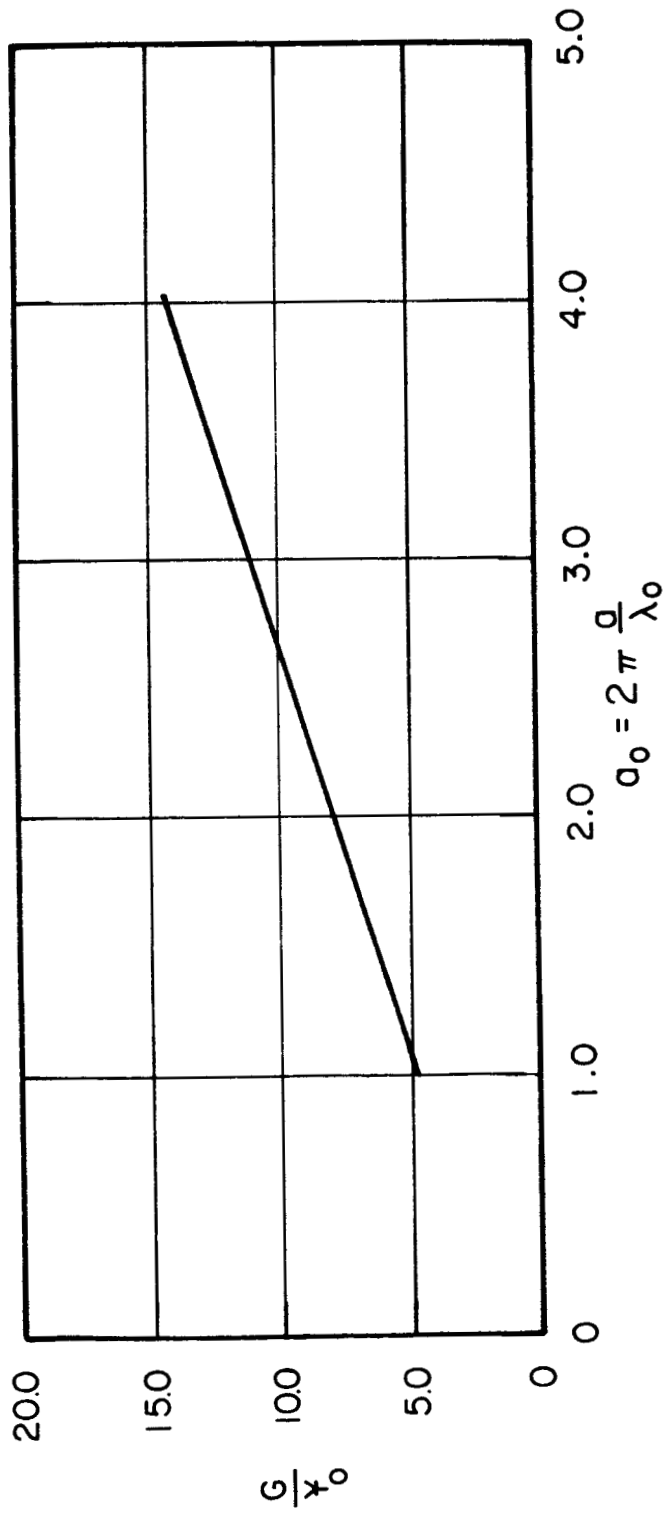
NASA

Figure 22.- Gap modal electric field distribution.



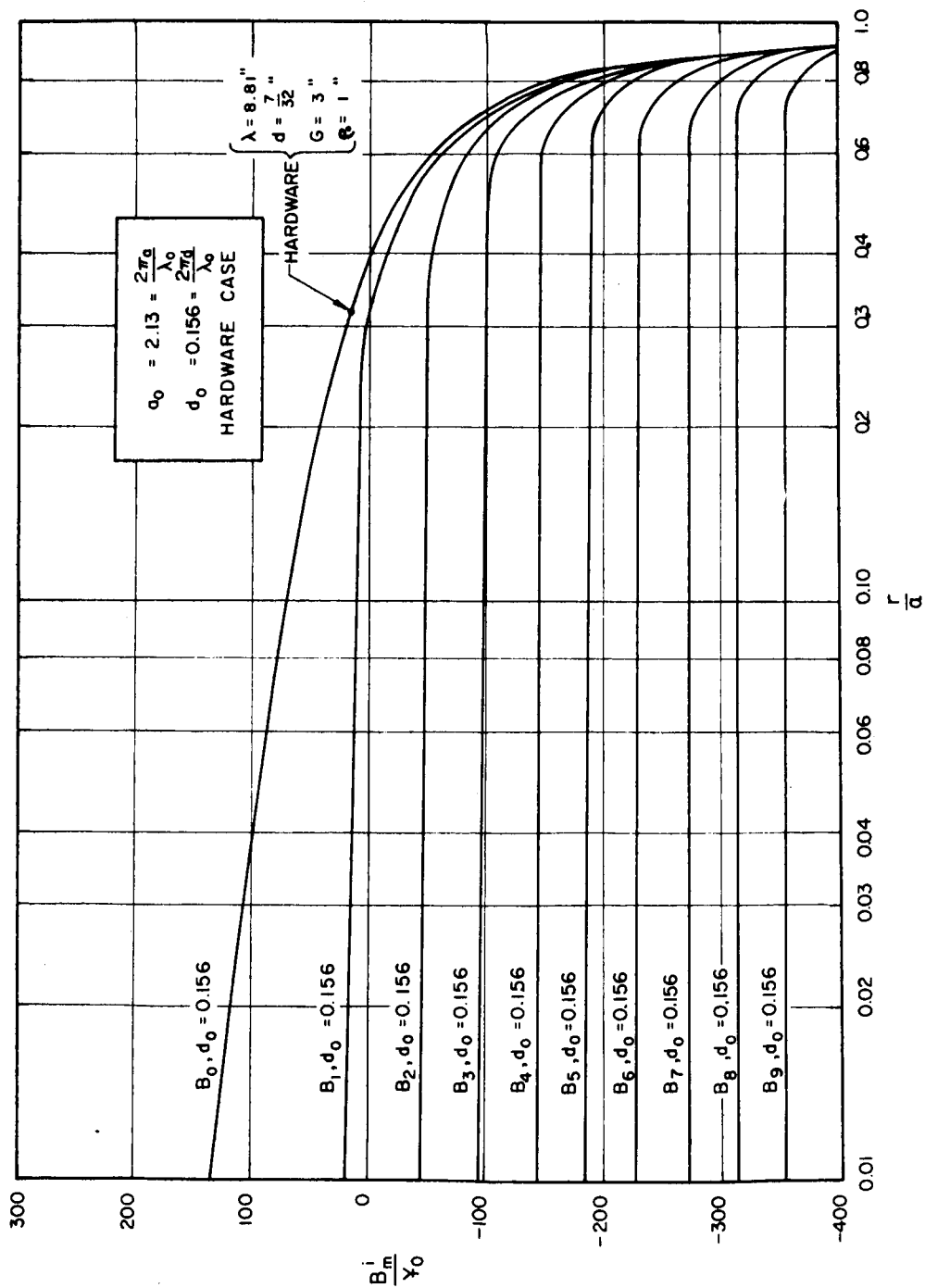
NASA

Figure 23.- Normalized aperture external susceptance as a function of cylinder circumference and gap width.



NASA

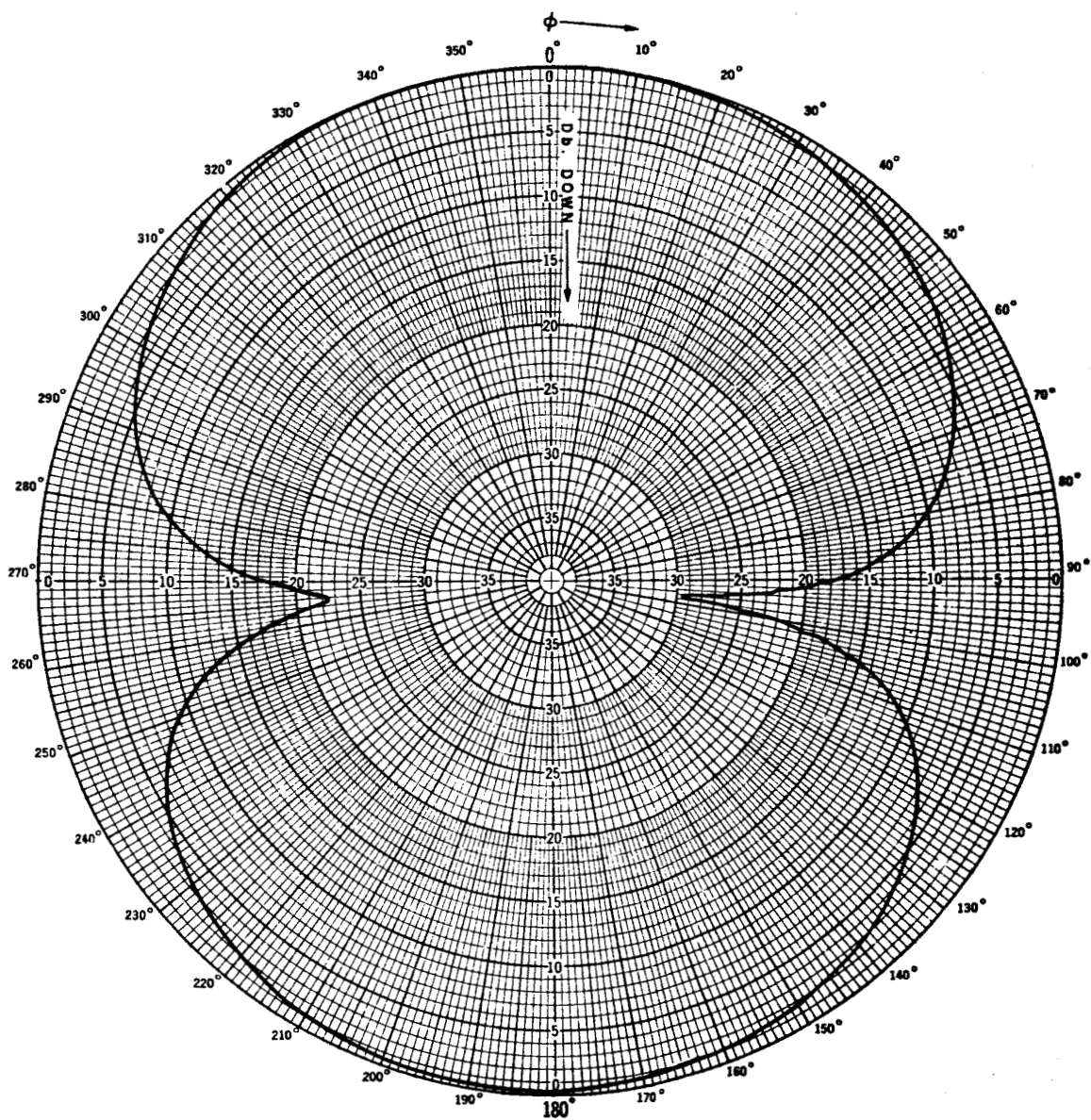
Figure 24.- Normalized aperture input conductance vs. cylinder circumference in wavelengths.



NASA

Figure 25.- Internal susceptance of gap antenna as a function of  $r/a$ .





NASA

Figure 26.- Measured equatorial pattern of gap antenna.